CRYSTAL GROWTH & DESIGN

pubs.acs.org/crystal

Article

Conjugation of a Silver-Based Coordination Polymer with Curcumin: A New Case of an Inorganic Polymeric Co-crystal

Alessandra Crispini, Massimo La Deda, Giuseppe Di Maio, Nicolas Godbert, Antonio Tagarelli, Rosangela Elliani, Angela Candreva, Renata De Rose, Iolinda Aiello, Mario Amati, and Francesca Scarpelli*

Cite This: *Cryst. Growth Des.* 2023, 23, 3518−3534

Read Online

ACCESS | Metrics & More | Article Recommendations | Supporting Information

ABSTRACT: A new structural form of the already reported silver-based 1D coordination polymer (CP) $[(bpy)Ag(OTf)]_\infty$ (bpy = 2,2′-bipyridine; OTf = trifluoromethanesulfonate) has been synthesized and fully characterized through single-crystal and powder XRD, DSC, and FTIR analysis. The reaction of both structural forms of the Ag(I) CP with curcumin (curc) afforded the formation of a new solid form, specifically an inorganic polymeric co-crystal between curc and [(bpy)Ag (OTf)] in a 1: 4 molar ratio, respectively. The co-crystal has been characterized both in solution and in the solid state through ^{1}H NMR, PXRD, DSC, IR, and UV−vis spectroscopies. In addition, a thorough computational study has been carried out to reveal the possible interaction modes between the co-crystal components. The Ag(I) compounds here presented have been preliminarily tested for antimicrobial activity against *Staphylococcus aureus* and *Escherichia coli* strains, all showing promising results.

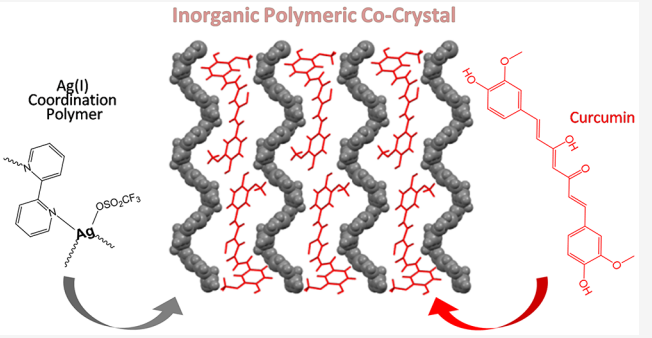

1. INTRODUCTION

Metallopolymers or metal-containing polymers (MPs) represent an innovative approach for the design of multifunctional macromolecular materials. Typically obtained by incorporating various metal centers (main-group metals, transition metals, and lanthanides) into an organic polymer backbone, MPs benefit from the properties of the polymeric frameworks and the functionalities of the metal centers, showing a notable range of applications in the field of material science, catalysis and bio-catalysis, environmental, and biomedicine.[1−6] Contextually, the field of MPs profited from the development of metal-mediated self-assembly as a tool to reach supramolecular metallopolymers.[7,8] The versatility of the strength and the number of metal−ligand interactions by varying the metal binding sites and the simple organic ligands has allowed the generation of one, two, or three-dimensional supramolecular metallopolymers, generally referred as coordination polymers (CPs), in particular, metal−organic frameworks (MOFs) or porous coordination polymers (PCPs) when porosity is present in the supramolecular network.[9,10] This new class of inorganic−organic hybrid materials has been recognized to possess a potential significant range of applications in antimicrobials, gas absorption and separation, luminescent materials, and drug delivery based on their different topologies and structures.[11−14] One-dimensional CPs, the simplest topological type of coordination arrangement, despite being considered the least structurally interesting, have received increasing attention due to the ease of synthesis and tunability of the resulting frameworks when compared to 3D CP structures.[15] Moreover, 1D CPs have shown a rich range of applications depending on the metal ions and the simple coordinating organic ligands, working as luminescent probes, dye adsorbers, and drug delivery systems.[16−18] In the case of silver-based CPs, the modulation of the dimensionality is well related to the variable coordination number and flexible geometries reached by this metal ion. Silver coordination compounds have received great attention owing to their appealing properties, in particular, their interesting biological activities.[19] Low toxicity, antimicrobial, anticancer, anti-inflammatory, antifungal, and antiplasmodial properties have been reported for many Ag(I) complexes.[20−24] In addition, the bacterial resistance to silver is rare and transitory;[24] thus, Ag(I) complexes could be considered as an alternative to common antibiotics against which resistant bacterial strains have developed. Moreover, the reaction between Ag(I) salts and

Received: January 11, 2023
Revised: March 31, 2023
Published: April 12, 2023

Downloaded via Mario Amati on May 5, 2023 at 13:03:52 (UTC).
See https://pubs.acs.org/sharingguidelines for options on how to legitimately share published articles.

ACS Publications

© 2023 American Chemical Society

https://doi.org/10.1021/acs.cgd.3c00042
Cryst. Growth Des. 2023, 23, 3518−3534

bridging bidentate ligands frequently affords the formation of 1D Ag(I) polymers, which can be considered excellent candidates as antibacterial agents.[25−30]

Recently, much attention has been focused on the preparation of co-crystals, which find application in the pharmaceutical and food sectors[31,32] as well as in the design of the next-generation electro-optical systems.[33−35] Generally, co-crystals are multicomponent crystalline materials composed of two or three small organic molecules. In addition, new categories of multicomponent crystals are currently under development. In particular, the rare polymeric co-crystals in which at least one component is a polymer are promising materials since the choice of a polymeric drug and/or co-former could represent an ingenious pharmaceutical strategy to modulate the stability, the solubility, and the release of poorly soluble drugs.[36−38] However, polymeric co-crystals as well as inorganic co-crystals have been infrequently obtained due to the fact that, in order to obtain a co-crystal, the starting materials should possess structural similarity, comparable potential energies, and almost identical crystallization kinetics.[39,40] Indeed, although a great number of organic co-crystals are known,[41] few examples of co-crystals including a metal complex have been reported so far.[42−48] Metal complexes with their precise geometries hardly exhibit lattice packing forces and crystallization kinetics similar to small organic compounds. Many examples of inorganic co-crystals are actually composed of two parent metal complexes[44,45] or geometrical isomers of the same coordination compound.[49]

In the past, we have been strongly involved in investigations concerning the formation of silver-based coordination compounds obtained through the interaction between the Ag(I) ion and 4,4′-disubstituted-2,2′-bipyridines where the careful choice of the substituents on the bipyridyl ligand and the nature of the counterions played a fundamental role in the modulation of the desired properties, such as liquid crystallinity.[25,50] Moreover, the use of 2,2′-bipyridine (bpy) in combination with silver salts in a 1:1 molar ratio has highlighted that the anion drove the coordination mode of the nitrogen ligand, giving rise to structures ranging from a discrete molecule to 1D CPs.[25,51] Continuing to explore the ability of bpy to generate 1D silver-based CPs as a ligand less investigated when compared with typical bipyridinium-bearing ligands used in the synthesis of CPs,[52] herein, we report the synthesis and the characterization of a new structural form ($\{[(bpy)Ag][OTf]\}_\infty$, hereafter referred to as the β-form) of the chiral silver-based coordination polymer of formula $[(bpy)Ag(OTf)]_\infty$ (hereafter referred to as the α-form) previously reported.[25] The two forms, namely, α and β, are characterized by the same building blocks but display a different arrangement of them, thus representing two structural isomers.

Both isomeric forms of the Ag(I) polymer have been used to explore their ability to accommodate organic molecules through non-covalent interactions, co-crystallizing, in particular, curcumin (curc), which is a fascinating molecule showing several beneficial properties to human health[53−55] and, most importantly, a very low tendency to coordinate the Ag(I) ion. This polyphenol for which in the solid state three different polymorphs (forms I, II, and III) are known[56] is characterized by poor bioavailability and low stability in solution, which are aspects that can both be overcome with the formation of co-crystals.[57−60] The best reaction conditions for the preparation of a binary $[(bpy)Ag(OTf)]_\infty$-curc co-crystal have been searched and found considering the difficulties related to both the formation of Ag(0) as a side event in the reaction between the Ag(I) polymer and curc polyphenol and the limited number of intermolecular sites on the Ag(I) polymer. The new $[(bpy)Ag(OTf)]_\infty$-curc species has been characterized through powder X-ray diffraction (PXRD), differential scanning calorimetry (DSC), FTIR, and UV−vis spectroscopies, while theoretical investigation has been performed to determine the possible interaction modes between the co-crystal components. Moreover, both Ag(I) polymeric forms and the $[(bpy)Ag(OTf)]_\infty$-curc co-crystal have been preliminarily tested for antimicrobial activity against *Staphylococcus aureus* (*S. aureus*) and *Escherichia coli* (*E. coli*) strains as models for Gram-positive and Gram-negative bacteria, respectively, with all showing promising results.

2. EXPERIMENTAL SECTION

2.1. Materials. All commercially available starting materials were used as received without further purification. Silver trifluoromethansulfonate (≥99%; AgOTf), 2,2′-bypiridine (≥99%; bpy), and ethylcellulose (EC; degree of substitution equal to 48.0−49.5% *w*/*w*) were purchased from Sigma-Aldrich. Curcumin (98%; curc, 1,7-bis(4-hydroxy-3-methoxyphenyl)-1,6-heptadiene-3,5-dion) was purchased from Carbosynth. ^{1}H NMR spectra were acquired on a Bruker Advance 300 MHz spectrometer in $CDCl_3$ solution (with TMS as the internal standard). FTIR spectra (KBr) in the range of 4000−400 cm^{-1} were recorded with a Spectrum One FT-IR PerkinElmer spectrometer. Elemental analyses were performed with a PerkinElmer 2400 microanalyzer. Powder X-ray diffraction patterns of the powder samples were acquired on a Bruker D2 Phaser equipped with Cu Kα radiation (λ = 1.5418 Å) and a Lynxeye detector at 30 kV and 10 mA with a step size of 0.01° (2θ). The obtained diffractograms were analyzed with DIFFRAC.EVA diffraction software. DSC analysis was performed on a DSC Q2000 TA instrument. The samples were accurately weighed (1.5−2 mg) and crimped in non-hermetic aluminum pans. The samples were heated at a heating rate of 5 °C min^{-1} under a dry nitrogen atmosphere (flow rate of 50 mL min^{-1}) using an empty non-hermetic aluminum pan as reference.

2.2. X-ray Crystallographic Analysis. Single crystal X-ray diffraction data of the β-form of $\{[(bpy)Ag][OTf]\}_\infty$ were collected at room temperature with a Bruker-Nonius X8APEXII CCD area detector system equipped with a graphite monochromator with radiation Mo Kα (λ = 0.71073 Å). Data were processed through SAINT reduction and SADABS absorption software.[61,62] The structure was solved by direct methods and refined by full-matrix least squares based on F^2 through the SHELX and SHELXTL software package.[63,64]

The carbon, sulfur, and oxygen atoms of the OTf anion are found to be disordered (named as C11A, S1A, F1A, F2A, F3A, and O3A). The relative occupancies of the two disordered components were refined freely while constraining their sum to unity,[65] and they reached values of approximately 0.77 and 0.23 at convergence. All non-hydrogen atoms were refined anisotropically and hydrogen atoms were included as idealized riding atoms. All graphical representations have been obtained using Olex2[66] and CCDC Mercury 4.3.0.[67] Details of data and structure refinements are reported in Table S1.

2.3. Synthesis of α-$[(bpy)Ag(OTf)]_\infty$. The α-form of the Ag(I) polymer was synthesized according to the procedure reported.[25] Specifically, bpy (150 mg, 0.96 mmol) was added to a degassed $CHCl_3$ solution of AgOTf (246.7 mg, 0.96 mmol). The resulting solution was stirred in the dark at room temperature and under an inert atmosphere (N_2). After 12 h, a white solid was recovered through filtration and recrystallized from CH_2Cl_2/diethyl ether. Yield: 68%, 270 mg; m.p. 168 °C. Anal. calcd for $[C_{11}H_8AgF_3N_2O_3S]$ (MW 413.12 g mol^{-1}): C 31.98, H 1.95, N 6.78%. Found: C 31.83, H 1.75, N 6.67%. ^{1}H NMR (300 MHz, $CDCl_3$ TMS), δ (ppm): 8.69 (d, J = 5.0 Hz, 2 H); 8.25 (d, J = 7.9 Hz, 2H); 8.06 (td, J = 7.6 Hz; 1.8 Hz, 2

https://doi.org/10.1021/acs.cgd.3c00042
Cryst. Growth Des. 2023, 23, 3518−3534

H); 7.57 (m, 2 H). FTIR (KBr cm^{-1}): 3066, 1590, 1472, 1438, 1254, 1168, 1032.

2.4. Synthesis of β-{[(bpy)Ag][OTf]}$_\infty$. To ca. 30 mL of a degassed $CHCl_3$ solution of bpy (150 mg, 0.96 mmol) was added AgOTf (246.7 mg, 0.96 mmol). The reaction mixture was stirred at room temperature under an inert atmosphere (N_2) and protected from light. After 12 h, a white solid was recovered through filtration and recrystallized from CH_2Cl_2/diethyl ether. Yield: 80%, 316 mg; m.p. 155 °C. Anal. calcd for $[C_{11}H_8AgF_3N_2O_3S]$ (MW 413.12 g mol^{-1}): C 31.98, H 1.95, N 6.78%. Found: C 31.87, H 1.82, N 6.82%. ^{1}H NMR (300 MHz, $CDCl_3$, TMS), δ (ppm): 8.80 (d, J = 4.8, 2H), 8.18 (d, J = 8.0 Hz, 2H), 8.04 (td, J = 7.8; 1.6 Hz, 2H), 7.59 (td, J = 6.7; 1.7, 2H). FTIR (KBr cm^{-1}): 3067, 1589, 1469, 1259, 1244, 1155, 1028. Single crystals were obtained by dissolving a few milligrams of the powder in hot $CHCl_3$ and letting the solution rest at room temperature for several days.

2.5. Preparation of 1a. A degassed MeOH solution of curc (142 mg, 0.39 mmol), protected from light was added to a degassed (N_2) MeOH solution of the Ag(I) polymer (α- or β-form; 160 mg, 0.39 mmol) in MeOH, protected from light. The resulting mixture was stirred at room temperature in the dark and under an inert atmosphere for 2 h. After this time, the reaction mixture was filtered through celite and concentrated through a rotavapor. A dark yellow precipitate (40 mg) obtained upon the addition of diethyl ether was recovered through filtration.

2.6. Preparation of 1. To a solution of curc (136 mg, 0.37 mmol) in MeOH was rapidly added KOH (20.7 mg, 0.37 mmol) under an inert atmosphere (N_2), keeping the reaction vessel protected from light. After a few minutes, this solution was added to a degassed (N_2) solution of the Ag(I) polymer (α- or β-form; 152 mg, 0.37 mmol) in MeOH, protected from light. The resulting mixture was stirred at room temperature in the dark and under an inert atmosphere for 2 h. After this time, the reaction mixture was filtered through celite and concentrated through a rotavapor. A red precipitate obtained upon the addition of diethyl ether was recovered through filtration. Yield: 80%, 150 mg; m.p. 142 °C. ^{1}H NMR (300 MHz, $CDCl_3$, TMS), δ (ppm): 8.67 (d, J = 6.8, 8H), 8.34 (d, J = 8.0 Hz, 8H), 8.03 (td, J = 6; 1.7 Hz, 8H), 7.55 (m, 10H), 7.14 (dd, J = 6.4; 1.7 Hz, 2H), 7.05 (m, 2H), 6.94 (d, J = 8 Hz, 2H), 6.48 (d, J = 15 Hz, 2H), 5.89 (s, 2H), 5.80 (s, 1H), 3.95 (s, 6H). IR (KBr cm^{-1}): 3420, 2916, 1626, 1592, 1514, 1263, 1229, 1169, 1033.

2.7. UV−Vis Characterization. Spectrofluorimetric grade CH_2Cl_2 was used for the photophysical investigations in solution. As previously reported,[68] a PerkinElmer Lambda 900 spectrophotometer was employed to obtain the UV−vis absorption spectra, a PerkinElmer LS 50B spectrofluorometer was used to obtain the emission spectra in solution, and in both cases, quartz cuvettes of a 1 cm path length were used.

Solid-state emission spectra were recorded on a Horiba Jobin Yvon Fluorolog 3 spectrofluorometer equipped with a Hamamatsu R-928 photomultiplier tube, and samples were prepared by placing a given amount of powder between two quartz slides and standardizing the layer.

2.8. Antibacterial Activity. The antibacterial activity of the two structural forms of the Ag(I) polymer, the co-crystal [(bpy)Ag]OTf$_\infty$-curc, and curc was tested against two bacterial strains, namely, *S. aureus* (DSM 346) as a model for Gram-positive bacteria and *E. coli* (DSM 1576) as a model for Gram-negative bacteria from DSMZ (German Collection of Microorganisms and Cell Cultures, Braunschweig). The lyophilized microorganisms were pre-cultured aerobically in 50 mL of DSM Medium 1 for *E. coli* and DSM Medium 92 for *S. aureus* for 18/24 h at 37 °C. The bacteria were maintained on a slant of nutrient agar (0.5% beef extract, 1% peptone, 0.5% NaCl, and 1.5% agar) at 4 °C and subcultured at regular intervals of 30 days to maintain the cell viability. For the preparation of microorganism suspensions, each bacterium was transferred from a stored slant to 10 mL of nutrient broth (meat extract, peptone, and NaCl) and cultivated overnight at 37 °C. The bacterial cultures were then diluted in sterile saline solution (0.9% NaCl) and adjusted to a cell suspension of 10^8 cells mL^{-1} using a UV spectrophotometer. The concentrations of bacteria were determined by measuring the optical density (OD) at 600 nm. Typically, for *E. coli*, an $OD_{600\ nm}$ of 0.1 corresponds to a concentration of 10^8 cells mL^{-1}.

Two milligrams of each sample (curc, α-[(bpy)Ag(OTf)]$_\infty$, β-{[(bpy)Ag][OTf]}$_\infty$, and [(bpy)Ag]OTf$_\infty$-curc) were mixed and finely ground with 100 mg of EC used as a diluting agent then pressed into pellets. A pellet containing only EC (EC0) was also prepared and used as the negative control.

The antibacterial activity of each sample was evaluated using the growth inhibition assay. The inhibitory effect of each compound on the growth of *S. aureus* and *E. coli* over 24 h of contact was evaluated by determining the number of viable bacteria for each specimen (CFU mL^{-1}). The pellets were placed in Petri dishes and immersed in 10 mL of a nutrient broth diluted 1:500 with the addition of the microorganism suspension at 10^6 cells mL^{-1} and incubated for 24 h at 35 °C in a humid environment. After this time, the inoculum was recovered and the dishes were washed with 10 mL of SCDLP broth, a neutralizer. The solutions were collected, and the microbial concentrations were determined by plating 100 μL of the appropriate dilution over the surface of the nutritive agar using a sterile bent plastic rod. All agar plates were incubated at 35 °C for 24 h with 95% humidity, and then, for each test specimen, the number of viable bacteria recovered after 24 h was determined. Each experiment was performed in duplicate and repeated four times for each test strain. The inhibitory effect was calculated using the following formula:

$$\text{percent inhibition} = 1 - T/C \times 100$$

where T is the CFU per milliliter of the test sample after 24 h, and C is the CFU per milliliter of the control (EC0) after 24 h. Generally, the bactericidal effect is obtained with a lethality percentage of 90% for 6 h, which is equivalent to 99% of lethality for 24 h.

2.9. Release Test for the Specific Migration of Ag(I) from the EC Tablet. The release of silver from tablets was measured by inductively coupled plasma−mass spectrometry (ICP-MS) analysis. The determinations were carried out utilizing an Elan DRC-e ICP-MS instrument (PerkinElmer SCIEX, Canada), and the sample delivery system consisted of a PerkinElmer autosampler model AS-93 Plus with a peristaltic pump and a cross-flow nebulizer with a Scott-type spray chamber. The ICP torch was a standard torch (Fassel-type torch) with a platinum injector. A solution containing Rh, Mg, Pb, Ba, and Ce (10 μg L^{-1}, Merck) was used to optimize the instrument in terms of sensitivity, resolution, and mass calibration. A multi-element solution containing Ag (100 mg/L, Merck) was used for the preparation of aqueous calibration standard solutions after appropriate dilution.

To evaluate the release of silver in physiological conditions, a tablet of α-[(bpy)Ag(OTf)]$_\infty$, β-{[(bpy)Ag][OTf]}$_\infty$, and [(bpy)Ag(OTf)]$_\infty$-curc was immersed in 10 mL of 0.9% NaCl solution at 37 °C. The release from each tablet was tested two times on contact: 6 and 24 h. After the time has elapsed, the tablet was removed, 100 μL of HNO_3 65% was added to the solution, and ICP-MS analysis was carried out. Each experiment was performed in duplicate.

2.10. Computational Methods. Gaussian 09, version D01,[69] was used for the structure optimizations of adducts between curcumin and Ag(I)-containing coordination units. A preliminary screening of all the possible adducts were performed with the use of the B3LYP xc functional[70] and def2-SVP basis set on all the atoms plus the related ECP on Ag only.[71] Such a survey of possible adducts is reported in the Supporting Information; in it, model systems were used in place of the real [(bpy)Ag(OTf)]$_\infty$ polymer: [(py)$_2$Ag]$^+$ and [(py)$_2$Ag][OTf] were placed in proximity of possible coordinating atoms of curcumin and full optimizations were performed starting from these choices. Adducts sketched in Figure 10 were found to be the most stable in which curc is in its EK and KK forms; they were refined by the means of full-structure optimizations with the same B3LYP xc functional and the more extended def2-TZP basis set and related ECP on Ag.[71] Default thresholds were used for structure optimizations and SCF computations. Integration grids were enhanced with the "int = ultrafine" keyword. The reported energies in Figure 10 are relative energies of the sketched structures with respect to their relaxed

https://doi.org/10.1021/acs.cgd.3c00042
Cryst. Growth Des. 2023, 23, 3518−3534

fragments, that is, relaxed curc and $[(py)_2Ag]^+$ for EK-2, EK-3, and KK-2 and relaxed curc and $[(py)_2Ag(OTf)]$ for EK-4 and KK-3. By "relaxed curc", we mean the fully optimized EK-1 tautomer. In all the cases of full-structure optimization, an analytical evaluation of the Hessian was performed to ensure that minima points of the PES were reached.

The Amsterdam density functional (ADF) program, version 2019,[72−74] was used for the decomposition of the binding energy in EK-2 and EK-4 (values in Table 4). In these computations, relativistic effects were included though the zero-order regular approximation (ZORA).[75,76] The B3LYP xc functional and the ZORA/TZP basis set included in the software were chosen for consistency with the methods used in the other computations. The decomposition scheme implemented in the program resulted from the modification of Ziegler and Rauk[77] of the original Morokuma and Kitaura scheme.[78] According to this approach, the bonding energy between two fragments is decomposed in terms of the Pauli repulsion energy between fragments, electrostatic interaction energy, and finally, orbital interaction. The last one takes into account all the stabilizing modifications of the electron density when passing from isolated fragments to their adduct. As a result, it includes both charge-transfer effects from one fragment to the second one and changes inside each fragment (polarization) due to the interaction between fragments. The preparation energy is the energy loss due to fragment deformation from their relaxed structures (isolated molecules) to the structures they assume in the adduct. This destabilizing energy term (positive energy) is summed to the favorable bonding energy between interacting fragments (negative energy) for obtaining the total interaction energy (negative in stable adducts). This analysis was performed on the structure computed with Gaussian 09 software as presented above without any modification.

Interactions between couples of curc molecules in their crystals (forms I, II, and III) were obtained after partial optimizations in which the C and O atoms were frozen in their experimental structure (polymorph I in ref 56) and only the H atoms were fully optimized in their positions. In this respect, the interaction energies in Figure 11 (ΔE_{inter}) are the energy difference between the whole adduct ("couple" in the figure) and the sum of the energies of the two isolated molecules, each frozen in the structure of the same adduct. An initial study aimed to the choice of the best xc functional was performed; results of this study are reported in the Supporting Information. The MP2 (second order Møller−Plesset correlation-corrected energy) and def2-TZP basis sets were used as reference for computing the interaction energies in couples 1, 2, and 4 (Figure 11). The B3LYP and M06[79] xc functionals demonstrated to be not sufficiently accurate. On the contrary, adding empirical dispersion in the D3 Grimme's approximation[80] (B3LYP-D3 and M06-D3; the standard "empiricaldispesion = gd3" keyword was used) strongly improved their performances. The B3LYP-D3 xc functional was chosen as the DFT method in these studies, and the def2-TZP basis set was combined to it. Anharmonic OH stretching wavenumbers in Figure 11 and Table 5 were obtained through numerical differentiation along selected harmonic normal modes: the keyword "freq = (anharmonic, select anharmonic modes)" was used, and the OH stretching mode of interest was selected. Inclusion of additional modes (stretching and bending modes) of all the OH and CO bonds involved in each couple of Figure 11 did not produce significant changes (a few units of cm^{-1}) with respect to selecting the single stretching mode reported in the figure.

3. RESULTS AND DISCUSSION

3.1. Preparation and Characterization of $\{[(bpy)Ag][OTf]\}_\infty$ (β-Form). Considering the coordination versatility of the N^N ligand bpy with respect to the Ag(I) ion in the presence of trifluoromethanesulfonate (OTf) as a counterion, the synthesis of Ag(I) CPs is a delicate procedure since, as already demonstrated by Klausmeyer et al., a modification of the stoichiometric ratio between the N^N ligand and the silver precursor could lead to the formation of a discrete compound rather than a polymer.[51] Moreover, polymorphism is frequently encountered in Ag(I) coordination polymers[81−84] as a result of the structural flexibility of the polymeric chains. It is known that, in a given reaction, the addition sequence of the reagents can influence the formation of different polymorphs[85−87] probably as a consequence of different solubilization rates of the reagents. On this basis, to test the formation of possible different structural forms of (bpy-Ag(I)-OTf) CPs, the synthetic procedure previously reported for the preparation of the α derivative[25] has been modified by reversing the order of the reagents' addition, keeping unchanged the stoichiometric ratio between the precursors. In particular, the α-form of the Ag(I) polymer was originally prepared through the addition of the bpy ligand to a AgOTf chloroform solution. This synthetic method afforded the formation of a Ag(I) coordination polymer with an empirical formula $[(bpy)Ag(OTf)]$ in the asymmetric unit crystallized in the $P3_121$ space group.[25] In this structural form, all metal centers are coordinated to the OTf anions. The α-form was thus re-prepared and obtained as white crystalline powder, whose identity has been confirmed by comparison between its PXRD pattern and that calculated from single-crystal data deposited at the Cambridge Crystallographic Data Centre (CCDC; Figure S1a). Moreover, all the characterizations are consistent with those previously reported.[25]

By inverting the addition sequence of the reagents with respect to the synthesis of the α-form, a white crystalline powder has been isolated, whose characterization in solution by ^1H NMR spectroscopy has highlighted the formation of a different structural form. Indeed, the different chemical shifts of the bpy proton signals of this new form of the Ag(I) polymer, that is, the β-form (see the Experimental Section), with respect to that reported in the literature for the α-form[25] is an indication of the different chemical environments experienced by Ag(I) ions.

The PXRD pattern of the new Ag(I) polymer has been found to be different than that recorded from the α-form (Figure 1).

Furthermore, the FTIR spectrum of the β-form (Figure 2, black line) exhibits significant differences with respect to that of the α-form (Figure 2, red line), particularly in the frequency region in which the OTf vibration bands occur. As already reported for Ag(I) coordination polymers bearing OTf as a

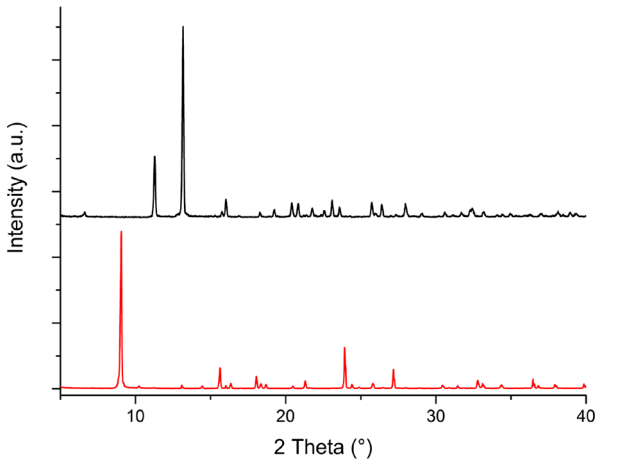

Figure 1. Comparison between the PXRD patterns of the α- (red) and β-form (black) of the Ag(I) polymer.

https://doi.org/10.1021/acs.cgd.3c00042
Cryst. Growth Des. 2023, 23, 3518−3534

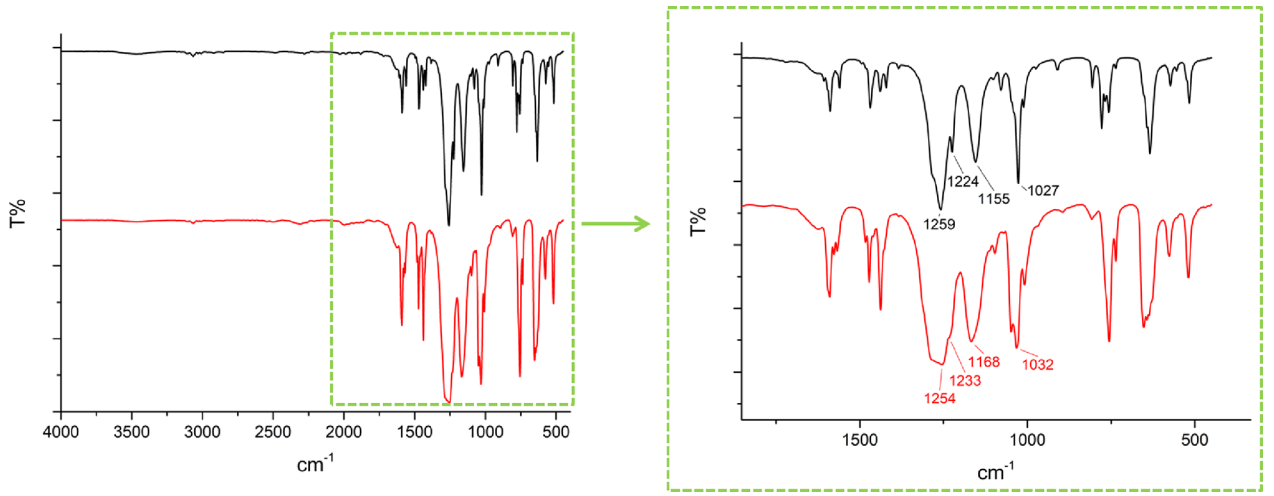

Figure 2. FTIR spectra of the α- (red) and β-form (black) of the Ag(I) polymer.

counterion,[88] the FTIR absorption bands of the OTf group could appear at different wavenumber values depending on whether or not the anion is coordinated to the metal ion. In the FTIR spectrum of the α-form, the bands attributed to the symmetric and asymmetric stretching of $-SO_3$ and $-CF_3$ groups, respectively, occur at 1032 and at 1168 cm^{-1}. These two vibration bands move to lower wavenumbers (1027 and 1155 cm^{-1}, respectively) in the FTIR spectrum of the β-form, suggesting the different interaction mode of OTf with the metal ion.

The thermal behavior of the β-form of the Ag(I) polymer was investigated through DSC and compared to that of the α-form. The DSC curve of the β-form (Figure 3, black line)

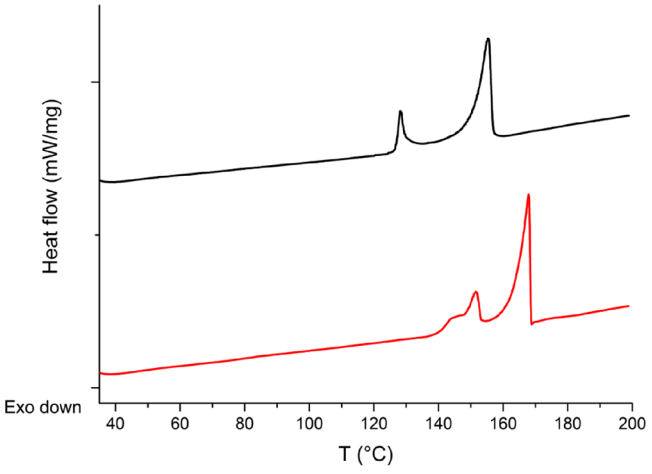

Figure 3. DSC curves of the α- (red) and β-form (black) of the Ag(I) polymer.

shows two thermal events: a solid−solid transition observed at 128 °C followed by the compound melting at 155 °C. The DSC trace of the α-form (Figure 3, red line) exhibits similar transitions to the β-form but at different temperature values; in particular, for the α-form, two very close solid−solid transitions occur at 144 °C ca. and 151 °C with the first appearing as a shoulder. The α-form melting is observed at 168 °C, revealing its higher thermal stability with respect to the β-form, probably deriving from greater lattice packing forces.

A molecular insight of the β-form was given by single crystal X-ray diffraction analysis performed on suitable single crystals grown from slow evaporation of a $CHCl_3$ solution of the powder sample. The β-form exhibits a polymeric structure but, differently from the α-form, presents an empirical formula [(bpy)Ag][OTf] in the asymmetric unit and crystallized in the $P2_1/c$ space group (Figure 4a). In the β-form, every Ag(I) ion is coordinated to the nitrogen atoms of two half bpy ligands, adopting a slightly distorted linear geometry (N(1)−Ag(1)−N(2) of 173.4(2)°). Bpy acts exclusively as a bridging ligand with a dihedral angle between the two aromatic rings of 52.2(2)°. As suggested by FTIR analysis, the OTf anions experience a different chemical environment with respect to the α-form; indeed, in the β-form, the OTf anions confined between the polymeric strands do not coordinate the silver centers (Figure 4a). The O(1) and O(2) atoms of each OTf anion weakly interact with two neighboring Ag(I) ions at distances of 2.951(6) and 2.798(5) Å, respectively, acting as a pincer-like anion and forcing the polymeric chains to adopt a zigzag conformation. As a consequence of this structural conformation, the O(3) atom of the OTf anion is found to be weakly interacting with the metal ion (distance of 3.12(1) Å). In the β-form, differently than what is observed in the α-form, no $\pi-\pi$ stacking between bpy ligands and no argentophilic interactions are present since the Ag···Ag distances are found to be of 5.320(1) Å. The additional intermolecular interactions found in the α-form whose structure is reported in Figure 4b could reflect the increased temperature values of the thermal events associated to the α-form.

The monophasic nature of the powder sample of β-$\{[(bpy)Ag][OTf]\}_\infty$ was confirmed by a comparison between the PXRD pattern measured on the powder sample and the simulated one derived from the single-crystal X-ray structure (Figure S1b).

3.2. Preparation and Characterization of the [(bpy)-Ag(OTf)]$_\infty$-curc Co-crystal. Recently, it has been reported that organic linear polymers can co-crystallize with small organic molecules by adjusting their conformation to accommodate a portion of the organic molecules.[36] Hence, both structural forms, α- and β-, of the Ag(I) polymer were used for the preparation of co-crystals with curc by virtue of their one-dimensional conformations, potentially capable of hosting the polyphenol. This approach is based on the idea to

https://doi.org/10.1021/acs.cgd.3c00042
Cryst. Growth Des. 2023, 23, 3518−3534

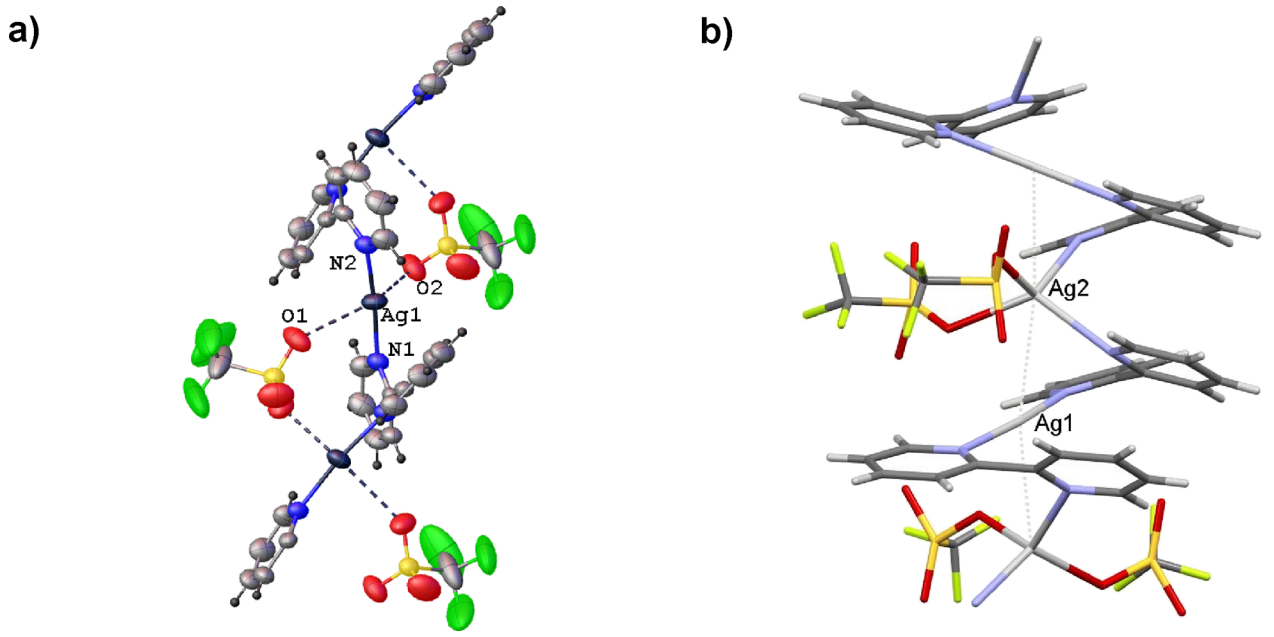

Figure 4. Perspective view of the β- (a) and α-form (b) of the Ag(I) polymer.

enhance the curc chemical stability and eventually bioavailability without its metalation to the Ag(I) centers, knowing that O,O-chelation to Ag(I) ions is highly improbable as testified by the presence of only one curc−Ag(I) complex in the literature.[89]

Considering that curc is generally prone to the formation of co-crystals through its keto-enolic and phenolic groups,[57,58,90,91] the formation of a Ag(I) polymer−curc co-crystal based on metal-to-oxygen intermolecular interactions could be expectable. However, since curc displays a certain tendency to reduce Ag(I) to Ag(0),[92−95] the formation of Ag(0) could happen as a side event in the reaction between the Ag(I) polymer and the polyphenol. Therefore, the preparation of $[(bpy)Ag(OTf)]_\infty$-curc co-crystals was attempted following two experimental conditions, namely, a neutral and an alkaline medium, in the search for the minimal reduction of Ag(I) to Ag(0). The basic conditions have been tried taking into account that (i) the reducing properties of curc are generally ascribed to its phenolic groups deprotonated in alkaline medium[96−98] and (ii) curc undergoes degradation much faster than under acidic/neutral conditions.[96,99]

The reactions between α-$[(bpy)Ag(OTf)]_\infty$ and β-$\{[(bpy)Ag][OTf]\}_\infty$ polymers and the form I of curc were first performed in the absence of a base. Both these reactions resulted in the formation of a significant amount of a dark-grey powder whose PXRD pattern is unequivocally attributable to the formation of zero-valence silver (Figure S2). Moreover, the same dark-yellow solid was recovered in a low yield from the filtrate of both reactions and analyzed through PXRD. The diffractogram of the yellow solid, referred as product **1a**, is characterized by a large and poorly resolved band in the 2θ range of 15−30° and a few diffraction peaks in the low-medium angle region, which are absent in the PXRD patterns of the precursors, which is thus diagnostic of the formation of a new product (Figure S3). However, this product has not been found to be a single species as evidenced by its DSC profile (Figure S4), which shows several thermal events. It is reasonable to assume that the poorly resolved PXRD pattern of product **1a** in addition to a new solid form also includes the diffraction peaks from other species.

The reactions between α-$[(bpy)Ag(OTf)]_\infty$ and β-$\{[(bpy)Ag][OTf]\}_\infty$ polymers and curc were subsequently performed in basic conditions. In this case, from both reactions, only a small amount of Ag(0) was formed and a pure red solid was recovered (see below DSC for purity). Both reactions yield the same solid, hereafter referred to as product **1**, as confirmed by PXRD analysis (Figure S5). This product was then characterized both in solution and in the solid-state. In particular, the ^{1}H NMR spectrum in solution (Figure S6) shows signals attributable to the free uncoordinated and fully protonated curc and the $[(bpy)Ag(OTf)]$ repetition unit of the Ag(I) polymer in a 1:4 ratio, respectively. This finding excludes the possibility of curc chelation to the metal center since the typical changes in the ^{1}H NMR chemical shifts of curc are not observed.[100,101] Moreover, in the ^{1}H NMR spectra of the new species, the bpy proton signals are observed at slightly different frequency values with respect to both the structural isomers of the Ag(I) polymer, indicating a possible structural change in the polymer. The full protonation of curc is also proved by SEM−EDX performed on product **1**, showing the complete absence of the potassium element. The PXRD analysis provided clear evidence of the formation of a new solid species. Indeed, the PXRD pattern of the new product is different from that of the pristine materials, curc, α-$[(bpy)Ag(OTf)]_\infty$, and β-$\{[(bpy)Ag][OTf]\}_\infty$ as evidenced in Figure 5. The diffractogram of product **1** (Figure 5, blue line) is characterized by the presence of new diffraction peaks, which are absent in the PXRD profiles of individual constituents (Figure 5, red, pink, and black lines) and, at the same time, by the absence of the distinctive reflections of the starting materials, pointing out the formation of a binary solid that is the $[(bpy)Ag(OTf)]_\infty$-curc co-crystal.

The formation of a new pure solid product was highlighted also by DSC analysis. Indeed, as shown in Figure 6, the thermal profile of product **1** ($[(bpy)Ag(OTf)]_\infty$-curc co-crystal, blue line) presents a single endothermic peak at 141.9 °C, thus at a temperature value different from the thermal

https://doi.org/10.1021/acs.cgd.3c00042
Cryst. Growth Des. 2023, 23, 3518−3534

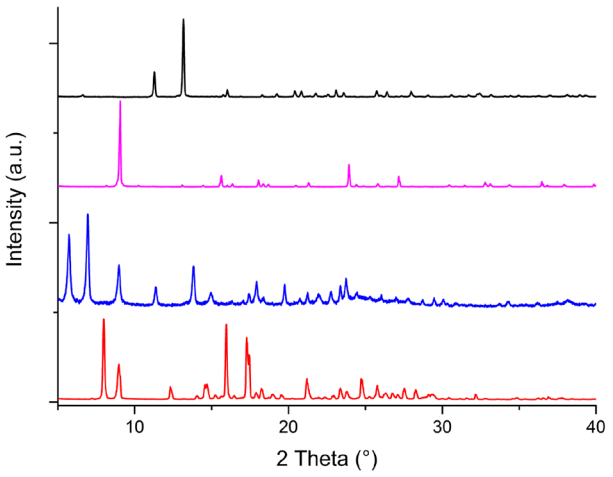

Figure 5. PXRD patterns of curc (red line), product **1** (blue line), α-[(bpy)Ag(OTf)]$_\infty$ (pink line), and β-{[(bpy)Ag][OTf]}$_\infty$ (black line).

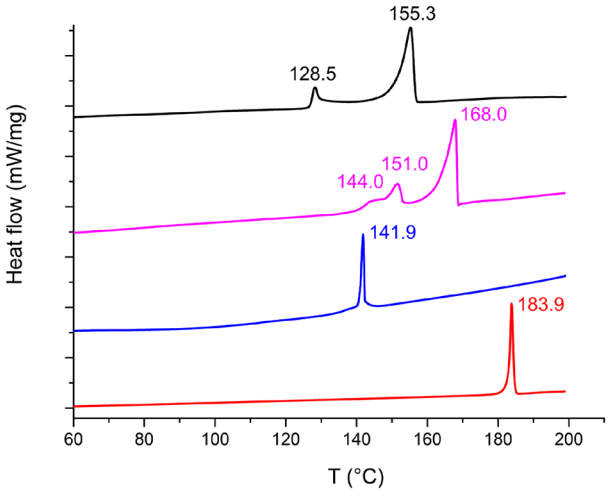

Figure 6. DSC curves of curc (red line), [(bpy)Ag(OTf)]$_\infty$-curc co-crystal (blue line), α-[(bpy)Ag(OTf)]$_\infty$ (pink line), and β-{[(bpy)Ag][OTf]}$_\infty$ (black line).

transitions of curc (red line), α-[(bpy)Ag(OTf)]$_\infty$, and β-{[(bpy)Ag][OTf]}$_\infty$ precursors (pink and black line, respectively). Hence, the peak at 141.9 °C, corresponding to the compound melting, is indicative of a homogeneous crystalline phase.

A careful comparison between product **1** and product **1a** highlighted the formation of the [(bpy)Ag(OTf)]$_\infty$-curc co-crystal even if in a low yield and not pure, also from the reaction carried out in the absence of a base. Indeed, in the PXRD pattern of product **1a**, the most intense reflections of the co-crystal are recognizable (Figure S7). In addition, in the DSC curve of product **1a** (Figure S3), the endothermic peak at 142 °C ca., which is attributable to the melting of the co-crystal, can be detected. However, in the absence of a base, the reaction between curc and the Ag(I) polymer mainly proceeds toward the formation of Ag(0). It can be hypothesized that the alkaline medium increases the speed of the process of curc degradation[96,99,102] particularly in the absence of stabilization through metalation of any deprotonated curc form, decreasing then the amount of curc available for the reduction of the Ag(I) ion in the polymeric system [(bpy)Ag(OTf)]$_\infty$.

Moreover, it should be noted that, whether starting from the α- or the β-form of the Ag(I) polymer, the same product is attained. This finding indicates that, when the Ag(I) polymer is mixed in solution with curc, a structural rearrangement occurs, allowing the formation of the same product despite the starting structural form of the Ag(I) polymer. FTIR analysis was performed to investigate the possible structural rearrangement of the Ag(I) polymer within the co-crystal. The FTIR spectrum of the co-crystal was thereby compared to the FTIR spectra of α-[(bpy)Ag(OTf)]$_\infty$, β-{[(bpy)Ag][OTf]}$_\infty$, and curc precursors (Figure 7). In the co-crystal spectrum (Figure 7, blue line), some bands of the starting precursors appear shifted (Table 1). In particular, in the FTIR spectrum of [(bpy)Ag(OTf)]$_\infty$-curc, the absorption bands resulting from the OTf vibrations (ν_{as} SO_3, ν_s SO_3, ν_{as} CF_3, and ν_s CF_3) all appear at higher frequency values with respect to the spectrum of the β-{[(bpy)Ag][OTf]}$_\infty$ form, while only the ν_{as} SO_3 and ν_s CF_3 bands are displaced with respect to the bands in the α-[(bpy)Ag(OTf)]$_\infty$ form (Table 1). This observation points out that, after the interaction with curc in the formation of the co-crystal, the structure of the Ag(I) polymer is more like the α-form than the β-form. Furthermore, differences

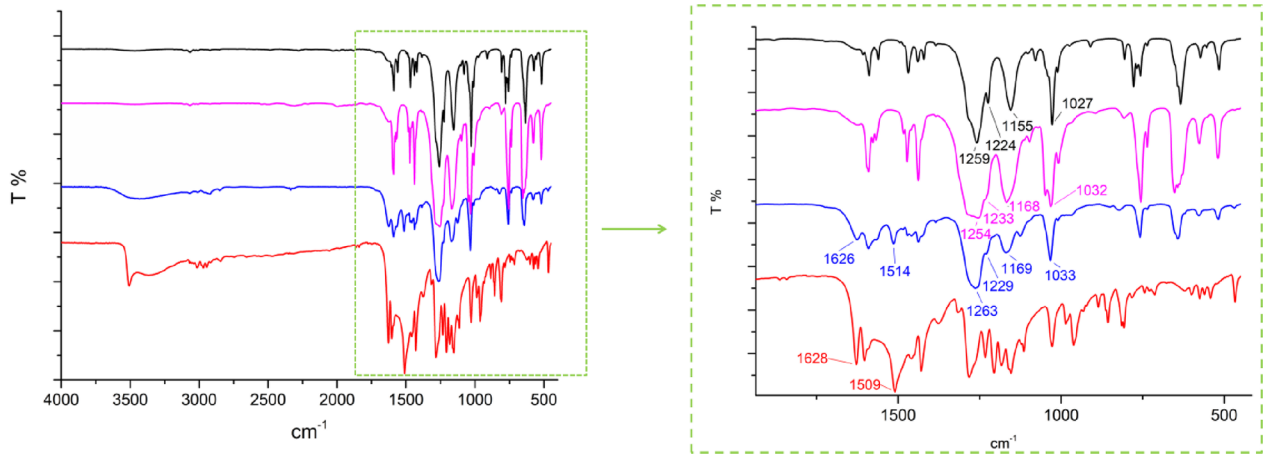

Figure 7. FTIR spectra of curc (red line), the [(bpy)Ag(OTf)]$_\infty$-curc co-crystal (blue line), α-[(bpy)Ag(OTf)]$_\infty$ (pink line), and β-{[(bpy)Ag][OTf]}$_\infty$ (black line).

https://doi.org/10.1021/acs.cgd.3c00042
Cryst. Growth Des. 2023, 23, 3518−3534

Table 1. FTIR Spectrum Data of curc, $[(bpy)Ag(OTf)]_\infty$-curc, and the Ag(I) Polymer (α- and β-Forms)

vibration	curc	$[(bpy)Ag(OTf)]_\infty$-curc	α-$[(bpy)Ag(OTf)]_\infty$	β-$\{[(bpy)Ag][OTf]\}_\infty$
νOH	3507, 3360 ca.	3440 ca.		
mixed νC=C/νC=O	1628	1626		
mixed νC=O/δC−C	1509	1514		
ν_{as} SO_3		1263	1254	1259
ν_s CF_3		1229	1233 (shoulder)	1224
ν_{as} CF_3		1169	1168	1155
ν_s SO_3		1033	1032	1027

emerge from the comparison between the FTIR spectra of curc and the co-crystal. In particular, the curc spectrum is characterized by a sharp peak at 3507 cm^{-1} and a broad band centered at 3360 cm^{-1} ca. with both arising from the stretching vibration of the hydroxyl groups.[103] Conversely, in the co-crystal spectrum, the O−H vibration generates a single broad band centered at 3440 cm^{-1} ca. The very large band at 2500 cm^{-1} ca. that is barely visible in the curc spectrum, which is attributable to the strong intramolecular hydrogen bonds of the enolic O−H,[104−106] disappears in the co-crystal spectrum. Moreover, the band at 1628 cm^{-1}, which is attributable to mixed νC=C/ νC=O vibrations of curc,[103] slightly shifts to a lower wavenumber (1626 cm^{-1}) in the FTIR spectrum of the co-crystal, whereas the band at 1509 cm^{-1}, due to mixed ν C=O/δ C−C vibrations of curc,[107] moves to higher wavenumber (1514 cm^{-1}) in the co-crystal spectrum. These findings indicate that both the keto-enolic function and the phenolic groups of curc could be involved in weak interactions with the Ag(I) polymer.

3.3. Photophysical Analysis. The photophysical analysis of the $[(bpy)Ag(OTf)]_\infty$-curc co-crystal was carried out both in the solid state and in CH_2Cl_2 dilute solution. The emission and excitation spectra of $[(bpy)Ag(OTf)]_\infty$-curc powder are reported in Figure 8. In the solid state $[(bpy)Ag(OTf)]_\infty$-curc

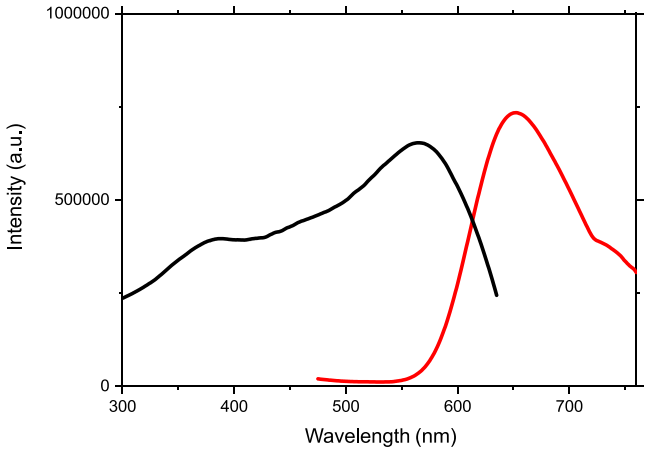

Figure 8. Emission (red line) and excitation (black line) spectra of the $[(bpy)Ag(OTf)]_\infty$-curc powder sample.

shows a single emission band centered at 655 nm with a shoulder at 730 nm. A comparison with emission and excitation spectra of the Ag(I) polymer (α- and β-form) and curc powders (Figures S8 and S9, respectively) confirms that a new chemical species that is different from its precursors is formed. Moreover, spectra reported in Figure S8 shows that α- and β-forms of the Ag(I) polymer have identical electronic transitions.

The absorption spectrum of $[(bpy)Ag(OTf)]_\infty$-curc in CH_2Cl_2 dilute solution (Figure 9, magenta line) shows a

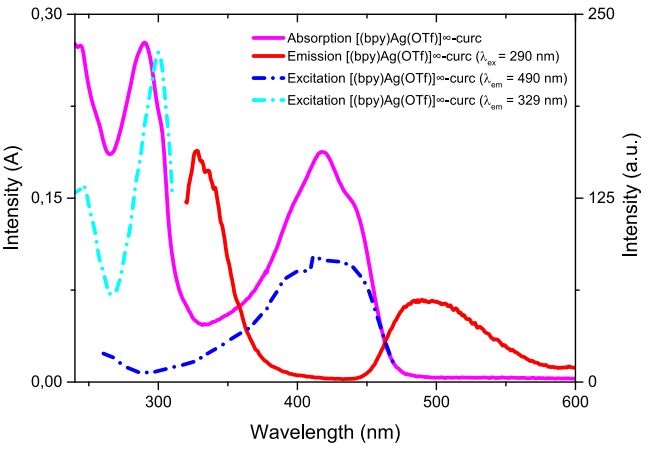

Figure 9. Absorption, emission, and excitation spectra of $[(bpy)Ag(OTf)]_\infty$-curc in CH_2Cl_2 dilute solution.

large band in the visible region of the electromagnetic spectrum with a maximum centered at 419 nm and two shoulders at 397 and 438 nm, respectively. Two further bands are visible in the UV region: a band centered at 290 nm with a shoulder at 302 nm and a band with a maximum at 247 nm and a shoulder at 256 nm. The comparison of this spectrum with the absorption spectra of curc (Figure S10, black line) and α/β-forms of the Ag(I) polymer (Figure S11, cyano and magenta lines, respectively) shows that the spectrum of the co-crystal in CH_2Cl_2 is exactly the sum of the absorption spectra of its constituents.

The emission and excitation spectra further confirm this statement. Exciting the co-crystal solution at 290 nm, two emission bands centered at 329 and 490 nm are obtained (Figure 9, red line). The blue-shifted emission and its corresponding excitation spectrum (Figure 9, cyano dot line) are like the absorption and emission features of the Ag(I) polymer (α- and β-form) (Figure S11), while the red-shifted one and its excitation spectrum (Figure 9, blue dot line) are similar to the absorption and emission spectra of curc (Figure S10).

Thus, while, in the solid state, the $[(bpy)Ag(OTf)]_\infty$-curc co-crystal maintains its integrity and only one emission signal is detected, in solution, a cleavage of the co-crystal superstructure takes place, resulting in the release of curc and $[(bpy)Ag(OTf)]_\infty$, and two different emission bands are detected.

3.4. Preliminary Antimicrobial Activity and Ag(I) Migration Test. Silver and its coordination compounds are known to show antimicrobial properties. In the case of Ag(I) complexes, different biological behaviors are related to

https://doi.org/10.1021/acs.cgd.3c00042
Cryst. Growth Des. 2023, 23, 3518−3534

Table 2. Antibacterial Activity (CFU Values) of α- and β-Forms of the Ag(I) Polymer, $[(bpy)Ag(OTf)]_\infty$-curc, curc, and EC0 and Relative Percentage of Growth Inhibition (%) against *S. aureus* and *E. coli*

sample	*S. aureus* CFU mL^{-1} after 24 h	percentage of growth inhibition	*E. coli* CFU mL^{-1} after 24 h	percentage of growth inhibition
EC0	3.2×10^8	0%	3.2×10^8	0%
α-$[(bpy)Ag(OTf)]_\infty$	≤1	100%	≤1	100%
β-$\{[(bpy)Ag][OTf]\}_\infty$	≤1	100%	≤1	100%
$[(bpy)Ag(OTf)]_\infty$-curc	4×10^3	99.9%	≤1	100%
curc	6.8×10^7	78%	13×10^7	60%

Table 3. Ag(I) Migration Expressed in Terms of Ag in Micrograms in 10 mL of Release from Pellets

time	α-$[(bpy)Ag(OTf)]_\infty$	β-$\{[(bpy)Ag][OTf]\}_\infty$	$[(bpy)Ag(OTf)]_\infty$-curc
6 h	2.8 ± 0.2	2.9 ± 0.2	3.6 ± 0.6
24 h	5.2 ± 0.7	4.9 ± 0.9	5.1 ± 0.7

different Ag(I)−ligand combinations, pointing out that the mere presence of silver is not sufficient for inducing antimicrobial activity.[108] Several works have been dedicated to explain that the bactericidal action of silver-based materials arises from the release of biocidal Ag(I) ions into the surrounding environment.[29,109] In an attempt to combine in one system the antimicrobial properties mainly expected from the silver polymer and the several biological activities carried by curc, here, the antibacterial performances of pellets containing the two structural forms α-$[(bpy)Ag(OTf)]_\infty$ and β-$\{[(bpy)Ag][OTf]\}_\infty$, the co-crystal $[(bpy)Ag(OTf)]_\infty$-curc, and curc were evaluated against *S. aureus* and *E. coli* microorganisms. Pellets were prepared using ethylcellulose (EC) powder as an inert diluting agent. Moreover, a pellet containing only EC (EC0) was tested as the negative control. The antibacterial activity of each compound was measured using the growth inhibition assay to count the colony forming units (CFUs) after 24 h of contact of the two microorganisms with the studied compounds. The results obtained by the growth inhibition assay are reported in Table 2.

The two structural forms α-$[(bpy)Ag(OTf)]_\infty$ and β-$\{[(bpy)Ag][OTf]\}_\infty$ display excellent bactericidal activity since, after 24 h of incubation, a total inhibition effect (100%) against both *S. aureus* and *E. coli* was registered. The same inhibition effect was measured for the co-crystal $[(bpy)Ag(OTf)]_\infty$-curc. Clearly, the high amount of the Ag(I) polymer used in the preparation of the samples does not allow either to differentiate the bactericidal activity against the two different microbial agents or to give a precise percentage of growth inhibition due to experimental limitation. However, the curc-containing pellets, although prepared with the same experimental condition used for the silver pellets, show only moderate antibacterial performance with respect to both *S. aureus* and *E. coli* microorganisms. Therefore, the high bactericidal effect observed for the co-crystal containing pellets could be only attributable to the presence of the Ag(I) polymer.

Moreover, to test the amount of silver ions released by each metal-charged EC pellet, Ag(I) migration has been tested in physiological conditions. In particular, the Ag(I) release was measured after 6 and 24 h of contact with a 0.9% NaCl solution at 37 °C. The overall Ag(I) migration values expressed in terms of micrograms per 10 mL of solution are reported in Table 3. Although after 6 h of contact, the release of Ag(I) is slightly greater from the tablet containing the co-crystal with respect to the ones containing the two isomers, while no relevant differences are observed between the three Ag(I) compounds after 24 h of contact. In all the tested tablets, despite the high quantity of Ag(I) compounds present (2 mg for each tablet), the Ag(I) release is very low with values of approximately 0.25% (w/w) after 24 h of contacts for all the tablets. These preliminarily results are encouraging for the possible use of these Ag(I) compounds as additives in antimicrobial polymeric carrier materials with a low metal release.

4. COMPUTATIONAL STUDY

In the absence of structural information on the co-crystal $[(bpy)Ag(OTf)]_\infty$-curc, a computational study in which several adducts between curc and $[(bpy)Ag(OTf)]_\infty$ were modeled was performed, aiming to suggest how the two components interact in setting up the co-crystal. The computational study was restricted at the interaction energy between the Ag(I) ion and curc with the silver centers in their low coordination number being the best interaction sites for the oxygen atoms of curc molecules. As a model system, the simpler $[(py)_2Ag]^+$ unit was used in the calculations in which two pyridine ligands coordinated to Ag(I) model the coordination of the two bridging bipyridines of the real polymer. The formation energy between curc and the Ag(I)-containing unit was calculated, as detailed in the Computational Methods. Some adducts are shown in Figure 10 together with their energies and other computed properties. Indeed, many further structures were optimized in which different curc conformations were considered and the OTf position was varied along with the Ag(I) coordination site. Many of the found structures are reported in the Supporting Information, while, herein, the most stable adducts and the most relevant ones are discussed. curc was considered both in its keto-enolic form (EK was used to label the different adducts associated with this curc tautomer) and diketonic form (named as KK). The KK tautomer was taken into consideration due to both experimental and computational evidence according to which the weak interaction between curc and external molecules (such as water) can make the KK form competitive with the EK ones.[110] In this sense, a coordination interaction with Ag(I) could impart a similar effect, potentially allowing the KK form to be present in the solid phase.

The energy difference between EK-1 and KK-1 (reported in Figure 10) is a measure of the stability gap between the two tautomers, which intrinsically originates in the single curc molecule. The calculated gap of 26.2 kJ/mol, in line with that reported in similar computational studies (24.6 kJ/mol[110] and

https://doi.org/10.1021/acs.cgd.3c00042
Cryst. Growth Des. 2023, 23, 3518−3534

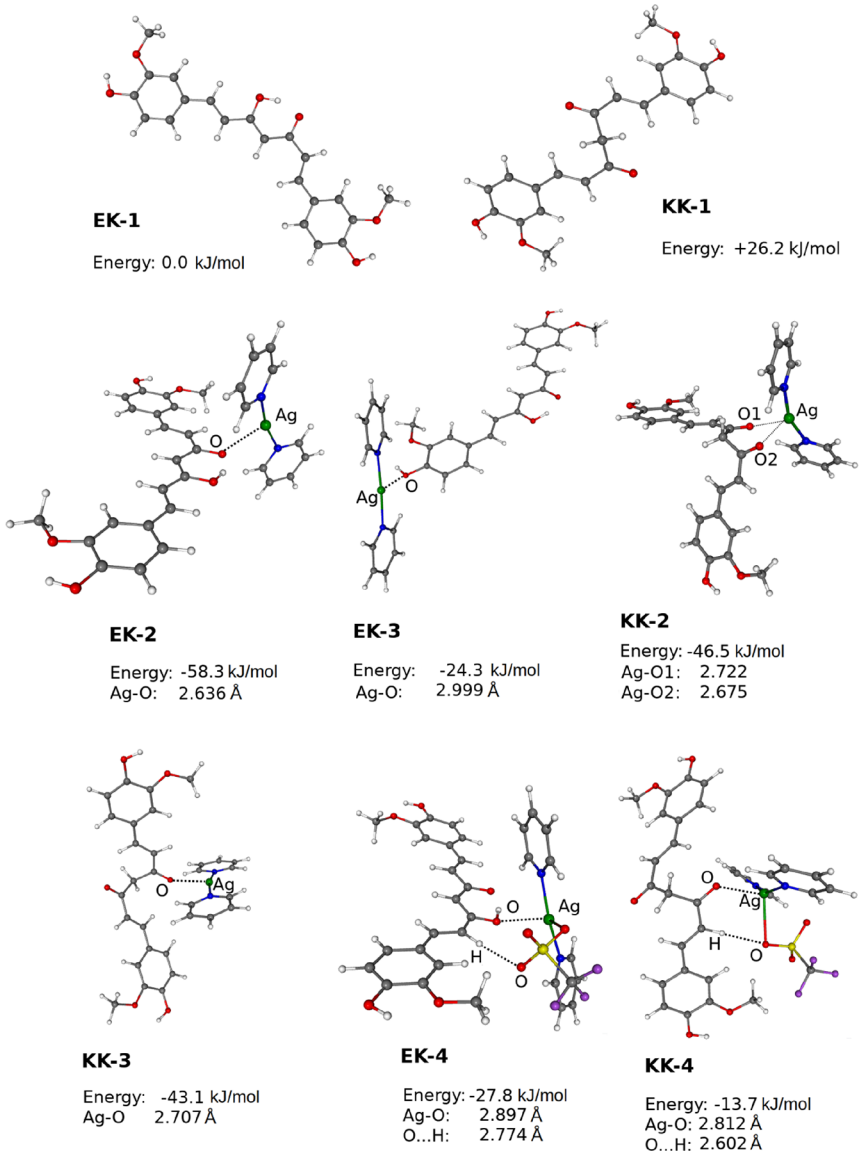

Figure 10. EK-1and KK-1 are the computed structures of curc in vacuum in its keto-enol and diketo forms, respectively. Their relative energies are reported (EK-1 is more stable); EK-2-3 and KK-2-3 are computed adducts between curc and $[(py)_2Ag]^+$. The reported energies are formation energies with respect to relaxed curc (EK-1 in all the four cases) and relaxed $[(py)_2Ag]^+$; EK-4 and KK-4 are the most stable adducts found between curc and $[(py)_2Ag][OTf]$. The reported energies are formation energies with respect to relaxed curc (EK-1) and relaxed $[(py)_2Ag][OTf]$.

~20 kJ/mol[111]), confirms the largely accepted higher stability of the EK form.

Considering all the computed adducts between $[(py)_2Ag]^+$and curc in its EK and KK forms (EK-2-3 and KK-2-3 in Figure 10), it is evident that the EK form still results as the most favored. EK-2 results indeed as the most stable adduct in which the Ag(I) ion interacts with the ketonic function of the EK curc moiety. Ag(I) interactions with the phenolic −OH and −OMe groups are much less effective as evidenced by the energy value of EK-3 in comparison with EK-2. The KK forms are not able to compete with the EK ones in terms of stability; KK-2 is the most stable structure found with curc in the KK form.

With the aim to include the possible effects due to the presence of the OTf counterion in the solid phase, adducts between curc and $[(py)_2Ag][OTf]$ were investigated. EK-4 and KK-4 were found to be the most stable structures (Figure 10) for the two curc tautomers. Evidently, the picture described above is not substantially changed. Likewise, the presence of a couple of $[(py)_2Ag]^+$ was additionally investigated and is described in the Supporting Information. In this case, in all the calculations, the EK form is found to be more stable with respect to the KK ones.

The Ag(I)−curc interaction was further investigated by means of the bonding energy decomposition scheme as implemented in the used ADF software, which is based on the Ziegler and Rauk modification of the Morokuma and Kitaura analysis of the bonding energy between interacting fragments (see the Computational Methods for details and references).

Table 4 collects the results of EK-2 and EK-4. In the first case, while curc and $[(py)_2Ag]^+$ are the two interacting fragments, in the EK-4 analysis, $[(py)_2Ag][OTf]$ is used as a metal-containing fragment. From the reported values, it appears evident that the orbital interaction term is important in establishing the bonding energy. However, it includes

https://doi.org/10.1021/acs.cgd.3c00042
Cryst. Growth Des. 2023, 23, 3518−3534

Table 4. Decomposition of the Bonding Energy between curc and $[(Py)_2Ag]^+$ in EK-2 and between curc and $[(py)_2Ag][OTf]$ in EK-3[a]

energy term	EK-2	EK-4
preparation Energy	+14.1	+23.0
steric repulsion (ΔE_{Pauli})	+72.8	+50.2
electrostatic interaction (ΔE_{elec})	−96.3	−74.0
total steric repulsion ($\Delta E_{Pauli} + \Delta E_{elec}$)	−23.5	−23.8
orbital interaction	−47.8	−26.7
total	−57.1	−27.0
curc charge	Mulliken: +0.06	Mulliken: +0.03
	Hirshfeld: +0.08	Hirshfeld: +0.02

[a]The ZORA/B3LYP/TZP approach was used. Values are in kJ/mol.

polarization effects inside the linked fragments and not only the charge transfer between them. Judging from the computed curc charge in the adduct, only a small amount of charge transfer is described from curc to the Ag(I)-containing fragment (0.06 and 0.03 electrons in EK-2 and EK-4 as estimated through the Mulliken scheme and 0.08 and 0.02 electrons estimated through the Hirshfeld charges, respectively). The lowering of charge transfer passing from EK-2 to EK-4 can be associated to the elongation of the Ag···O distance reported in Figure 10 and also to a reduction of curc polarization passing from the charged $[(py)_2Ag]^+$ to neutral $[(py)_2Ag]OTf$. Moreover, such a lower polarization seems to be mainly responsible for the smaller orbital interaction energy in EK-4 with respect to EK-2. This further supports the hypothesis of a general weak energy gain associated to a charge donation from curc to Ag(I).

From above, curc interacts with the Ag(I) ion mostly through an electrostatic interaction enhanced by polarization effects.

It is possible to summarize the data in Figure 10 and the discussion above with the following statements:

(a) **curc** is expected to maintain the EK form also following the coordination interaction with one or two Ag(I) ions.
(b) The EK-2 adduct (and the related EK-4) spots the more favorable curc interaction site for Ag(I); hence, it is the more worthy to be further investigated. In other words, curc first employs its keto-enolic function when interacting with the $[(bpy)Ag(OTf)]_\infty$ polymer.

With the aim to find experimental evidence of the second statement, FTIR spectra underwent a deeper investigation. In Section 3.2, the changes in the OH stretching bands were discussed (see Figure 7, Table 1, and related discussion). The very broad keto-enol OH stretching band is visible in the curc FTIR spectrum around 2500 cm^{-1} and disappears in the co-crystal. This evidence is a clue in favor of changes in the environment surrounding the curc EK core. In this sense, it could be ascribed to the establishment of the interaction with the Ag(I) center in the co-crystal. However, more insights were gathered from changes in the phenolic OH stretching bands.

As already discussed in Section 3.2, in the curc experimental FTIR spectrum, two bands were detected for the phenolic OH stretching mode at 3507 and ∼3360 cm^{-1}. The band at 3360 cm^{-1} is more intense and broader. This finding allows assigning the solid phase of curc under investigation to the polymorph I, which is the most stable crystalline phase reported to date.[56] The reported and less stable polymorph II shows two phenolic −OH peaks stretching bands as well, whereas form III only presents a single broad OH band (Table 5).[56]

The presence of two bands in the experimental FTIR spectrum of curc was also reported in KBr pellets[111] and is common in FTIR spectra of solid curc due to the higher stability of form I. On the contrary, in solution, a single phenolic OH band is visible: in CCl_4 and $CDCl_3$, sharp bands were reported at 3545 and 3536 cm^{-1}, respectively, which is considered diagnostic of the phenolic groups undergoing weak intramolecular H-bonds. Differently, in acetonitrile, a broader and more intense band at 3374 cm^{-1} was recorded, which is explained as a consequence of a strong H-bond with the solvent.[111] On this basis, we can infer that the two phenol rings of curc are differently involved in H-bonds and/or other interactions with neighboring molecules at least in the two polymorphs I and II.

With the aim to achieve a deeper comprehension, the interactions between adjacent molecules of curc in its polymorph I have been considered. Figure 11 shows couples of curc molecules, which are in contact in the crystal, resulting from the crystallographic analysis.[56] The computed interaction energies of each couple are shown in Figure 11 along with selected structural and spectroscopic data (see the Computational Methods for details about the used methods in the applied structure optimization). Inside the crystal, each curc molecule assumes a non-planar structure in its EK tautomeric form, differently from what is computed in the gas phase in this work and also computed in solution in previous reports.[110,111]

One of the two phenolic groups is clearly rotated with respect to the remaining structure (the keto-enolic central part and the co-planar second phenol ring; see Table 5 for further

Table 5. Experimental and Computed Phenolic OH Stretching Modes and curc Structural Distortion in the Three Polymorphs of Solid curc

crystal	curc distortion (degrees)[a]	experimental phenol νOH (cm^{-1})	computed phenol νOH (cm^{-1}) and their assignment
form I	46.8[a]	two bands: 3507; 3360[c]	3392, phenol−EK core H-bond[e]
		two bands: 3511; 3399[d]	3527−3533, phenol−phenol H-bond[f]
form II	17.0; 12.1[b]	two bands: 3254; 3401[d]	3197, phenol−EK core H-bond[g]
			3406, phenol−phenol H-bond[g]
form III	12.6[b]	one band: 3441[d]	3383, phenol−EK core H-bond[g]
			3432, phenol−phenol H-bond[g]

[a]Dihedral angle between the average plane of the distorted phenol ring (only the ring) and the average plane of the remaining of curc structure; only C and O atoms are used, methyl is fully excluded; experimental values are taken from ref 56. [b]Dihedral angle between the average plane of the distorted phenol ring plus the CHCH group directly connected to it and the average plane of the remaining of curc structure; only C and O atoms are used, methyl is fully excluded. [c]This work. [d]Ref 56. [e]Couple 1 in Figure 11. [f]Couple 3 in Figure 11. [g]See the Supporting Information for details.

https://doi.org/10.1021/acs.cgd.3c00042
Cryst. Growth Des. 2023, 23, 3518−3534

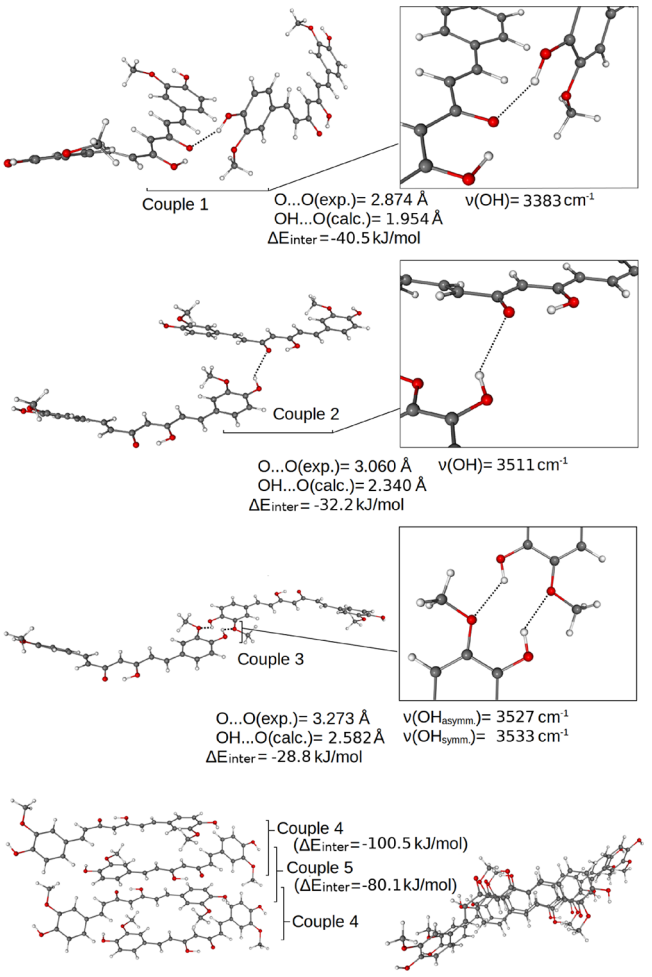

Figure 11. Couples of curc molecules found in contact in the form I crystal. Couples 1−3 model the H-bond contacts. Couples 4−5 alternate themselves to form an infinite monodimensional stack. Two views of a four-molecule part of the stack are sketched in bottom-right and left corners. See the Computational Methods for details on the listed interaction energies (ΔE_{inter}); ν(OH) is the stretching wavenumbers in the anharmonic approximations. In the case of couple 3, symmetric and asymmetric double-OH stretching modes are distinguished.

details). This distortion is to maximize the interaction between the phenolic OH group and the EK central moiety of the adjacent curc molecule. Such a contact is modeled by couple 1 in Figure 11, which shows the shorter of the experimental O···O distances, the shorter of the computed OH···O distances between all the H-bond-forming couples of adjacent molecules (couples 1−3 in Figure 11), and the stronger H-bond (ΔE_{inter} in Figure 11).

Couples 2 and 3 show longer O···O and OH···O distances in comparison to couple 1. They involve the phenolic group coplanar with the keto-enolic central part of the curc structure. Thus, the "distorted" phenol gives rise to the strongest H-bond (couple 1) and the consequently lower computed OH stretching wavelength with respect to couples 2 and 3 (Figure 11 and Table 5). The computed stretching frequency corrected for anharmonicity (ν_{anharm}) amounts to 3392 cm^{-1}. In couples 2 and 3, the same anharmonic wavelengths are calculated to be equal to 3511 and in the 3527−3533 cm^{-1} range, respectively, which is in line with calculations performed on a single curc molecule in vacuum (3538 and 3540 cm^{-1}; the two phenol rings are not symmetry-related) where only the intramolecular phenolic H-bond is present.

From above, our computations clearly assign the red-shifted IR band at ∼3360 cm^{-1} to the rotated phenol ring, which is the one undergoing the stronger H-bond with the EK core of the adjacent curcumin. The sharper and weaker band at 3507 cm^{-1} is assigned to the planar phenol ring, which is not interested in strong H-bond interactions (apart from the intramolecular H-bond). This is in perfect agreement with the previously discussed results on the IR spectra in solutions with different abilities to form H-bonds.

Interestingly, the stronger interactions between curc molecules in the crystal are not H-bonds; rather, they are associated to stacks of almost parallel curc molecules described by couples 3 and 4 in Figure 11. Their interaction energies are largely superior to the ones in couples 1−3, and, in this light, the fact that similar stacks are also present in curc forms II and III can be easily explained. In forms II and III, H-bonds are also present, and they were studied by applying similar computational methods to form I. These results are discussed in the Supporting Information, here, we summarize some findings in Table 5 and in the short discussion below. In both the forms, a lower (but still present) distortion from planarity is present in the curc structure (Table 5). In form II, distorted (17.0°) curc molecules form H-bonds with the EK core of adjacent molecules in a similar way to couple 1 in form I. The resulting phenol OH-stretching mode is computed at 3197 cm^{-1}, which is very close to the experimental peak at 3254 cm^{-1} (Table 5). The other computed OH-stretching modes are associated to weaker phenol H-bonds and to the experimental band at 3401 cm^{-1}. In form III, curc shows a lower distortion from planarity (12.6°) and a weaker H-bond with the EK core of a second molecule. As a result, the related OH stretching mode shifts at 3383 cm^{-1} and overlaps with the OH-stretching bands of the other phenol rings (computationally estimated at 3432 cm^{-1}) to produce a single experimental band at 3441 cm^{-1}.

To summarize the discussion above, a clear correspondence is highlighted between the involvement of the phenol ring in H-bonds with the EK core of a second molecule and the presence of red-shifted bands in the zone of the phenol OH stretching. The point is that, as shown in Figure 7, passing from polymorph I of curc to the co-crystal, a single absorption band at ∼3440 cm^{-1} (blue spectrum) replaces the two peaks (red spectrum) of form I. This finding further confirms the change in the environment surrounding the EK function of curc, which can be easily referred to the interaction of the EK site with the Ag(I) ion. Comparing the computed formation energies of EK-2 and EK-4 (Figure 10) with the interaction energies of couple 1 (Figure 11), it appears evident that the Ag(I) interaction can replace the H-bond between adjacent molecules. On the contrary, the stacks of curc (couples 4 and 5) are expected to be preserved in the formation of the co-crystal owing to their strong interaction.

From above, it is possible to propose tentatively some basic structural characteristics of the $[(bpy)Ag(OTf)]_\infty$-curc co-crystal: during co-crystallization, the curc crystal packing is likely preserved in terms of the stack of parallel molecules (couples 4 and 5 in Figure 11, evolving in a similar pattern). The strong H-bond described by couple 1 in Figure 11 is replaced by the Ag(I) coordination interaction. Hence, curc loses the energetic drive for distorting itself from planarity and the two phenolic rings become more symmetric, giving rise to

https://doi.org/10.1021/acs.cgd.3c00042
Cryst. Growth Des. 2023, 23, 3518−3534

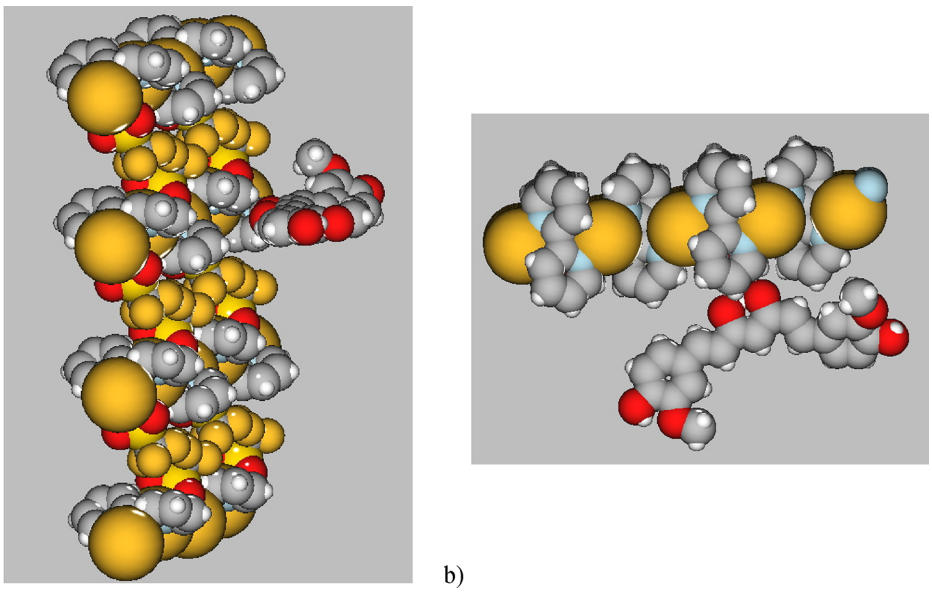

Figure 12. Proposed model for the curc-$[(bpy)Ag(OTf)]_\infty$ co-crystal pictured from two different viewpoints, showing (a) the proximity between curc and the $[(bpy)Ag]^+$ cationic chain and (b) the dimensionality ratio between curc and four $[(bpy)Ag]^+$ repeating units.

a single FTIR OH-stretching band. The co-crystal would result in a repetition of two domains: the curc domains (stacks) and adjacent $[(bpy)Ag(OTf)]_\infty$ domains (chains), interacting via coordination interactions between the curc EK moiety and one Ag(I) ion for every four in the crystal. Figure 12, which is obtained by extracting a part of the curc stack in its form I crystal[56] and a small part of the $[Ag(bpy)]^+_\infty$ chain from α-$[(bpy)Ag(OTf)]_\infty$, shows the proposed model for the $[(bpy)Ag(OTf)]_\infty$-curc co-crystal addressed to give a possible description of its crystal structure. Considering that the length of a single curc molecule of approximately 17 Å from the crystal structure in its polymorph I is comparable with the length of four $[(bpy)Ag]^+$ repeating units, it is reasonable to propose that not all the Ag(I) ions are involved in the curc coordination interactions and each curc molecule is surrounded by four Ag(I) metal ions, which is in agreement with the 1:4 ratio between curc and $[(bpy)Ag(OTf)]$ unit as evidenced by NMR measures in this work.

5. CONCLUSIONS

A new structural isomer (β-form) of the already reported Ag(I)-CP $[(bpy)Ag(OTf)]_\infty$ (α-form) has been synthetized and fully characterized. In particular, the β-form was obtained by inverting the sequence of the reagent's addition with respect to the synthesis of the α-form. Hence, the Ag(I) coordination versatility of the bpy ligand is demonstrated when a slight modification of the known synthetic procedure is sufficient to significantly modify the resulting coordination polymer, removing the spontaneous chiral resolution process occurring during crystallization observed in the α-form.

Both isomers of the Ag(I)-CP, α- and β-forms, by virtue of their flexible conformations and silver ions in a low coordination number were used in the preparation of co-crystals with curc (polymorph I). However, curc displays a certain tendency to reduce Ag(I) to Ag(0), which is reasonably ascribed to the reducing properties of the phenolic groups of the polyphenol. Hence, in the attempt to find the best conditions minimizing the formation of Ag(0), the reaction between the α- and β-forms of the Ag(I)-CP and curc was performed in the absence and presence of KOH. In both experimental conditions, a new solid form as evidenced by PXRD analysis was formed; however, in the absence of the base, the new solid form was obtained in a low yield and was not pure since the reaction between curc and the Ag(I) polymer mainly proceeds toward the formation of Ag(0). Therefore, the deprotonation of the phenolic moieties in KOH decreases the reactivity of curc toward the reduction of Ag(I) in the polymeric system $[(bpy)Ag(OTf)]_\infty$. The presence of protonated curc within the binary co-crystal even if obtained in alkaline conditions as well as the decreased reduction of Ag(I) to Ag(0) point out that the lack of chelation or any type of metal coordination of the anionic forms of curc allows for their fast degradation process toward degradation products less powerful as reducing agents. Indeed, the characterization of this new product highlighted the formation of a co-crystal composed of $[(bpy)Ag(OTf)]_\infty$ and curc, meaning a homogeneous crystalline phase in which there is no evidence of a proper metal coordination of curc. Moreover, as proven by the photophysical studies, in the solid state, the $[(bpy)Ag(OTf)]_\infty$-curc co-crystal maintains its integrity, showing distinctive emission and excitation spectra, whereas, in solution, a cleavage of the co-crystal superstructure takes place, resulting in the release of curc and $[(bpy)Ag(OTf)]_\infty$. A comprehensive computational study was performed to unveil the possible interaction modes between the co-crystal components. The theoretical analysis suggested that, within the co-crystal, curc maintains the EK form and the strong H-bond between the ketonic function and a phenolic group of curc observed in the crystal structure of polymorph I is replaced by a coordination interaction between the keto-enol moiety and Ag(I) ions. Finally, preliminary antimicrobial and release tests performed on EC pellets containing the Ag(I)-CP (α- or β-form), the co-crystal, and curc indicate the high antibacterial activity of the Ag(I)-based compounds with a low Ag(I) release. Although curc exhibits much lower antibacterial activity with respect to the Ag(I)-CPs, the co-crystal retains the high antimicrobial performance of the Ag(I) species. On this basis, the co-crystal could be considered to be a multifunc-

https://doi.org/10.1021/acs.cgd.3c00042
Cryst. Growth Des. 2023, 23, 3518−3534

tional system, potentially displaying the multiple properties of curc besides the antimicrobial activity typical of Ag compounds.

■ ASSOCIATED CONTENT

Supporting Information

The Supporting Information is available free of charge at https://pubs.acs.org/doi/10.1021/acs.cgd.3c00042.

Comparison between the PXRD patterns calculated from single-crystal data and those measured on powder samples for the α-form and β-form, crystallographic data for the β-form of $\{[(bpy)Ag][OTf]\}_\infty$, PXRD profile of the grey powder obtained as a byproduct in the preparation of **1a** compared with the Ag reference pattern, PXRD profile of product **1a** compared with curc, α-$[(bpy)Ag(OTf)]_\infty$, and β-$[(bpy)Ag][OTf]\}_\infty$ patterns, DSC curve of **1a**, PXRD profiles of product **1** (obtained from the reaction between the α-form and curc; obtained from the reaction between the β-form and curc), ^{1}H NMR spectrum in $CDCl_3$ of product **1**, comparison between PXRD patterns of compounds **1** and **1a**. Excitation and emission spectra of α- and β-form powders, excitation and emission spectra of curc powder, absorption and emission spectra of curc in CH_2Cl_2 solution, absorption and emission spectra of the Ag(I) polymer (α- and β-forms) in diluted CH_2Cl_2 solution, the chosen DFT method applied to the intermolecular interactions in solid curc, hydrogen bonds in curc forms II and III, and a survey on the studied curc−Ag(I) interaction (PDF)

Accession Codes

CCDC 2235451 contains the supplementary crystallographic data for this paper. These data can be obtained free of charge via www.ccdc.cam.ac.uk/data_request/cif, or by emailing data_request@ccdc.cam.ac.uk, or by contacting The Cambridge Crystallographic Data Centre, 12 Union Road, Cambridge CB2 1EZ, UK; fax: +44 1223 336033.

■ AUTHOR INFORMATION

Corresponding Author

Francesca Scarpelli − *MAT-InLAB, LASCAMM CR-INSTM, Unità INSTM della Calabria, Dipartimento di Chimica e Tecnologie Chimiche, Università della Calabria, 87036 Arcavacata di Rende, CS, Italy;* orcid.org/0000-0002-3461-0478; Email: francesca.scarpelli@unical.it

Authors

Alessandra Crispini − *MAT-InLAB, LASCAMM CR-INSTM, Unità INSTM della Calabria, Dipartimento di Chimica e Tecnologie Chimiche, Università della Calabria, 87036 Arcavacata di Rende, CS, Italy;* orcid.org/0000-0002-7522-9323

Massimo La Deda − *MAT-InLAB, LASCAMM CR-INSTM, Unità INSTM della Calabria, Dipartimento di Chimica e Tecnologie Chimiche and CNR-NANOTEC, Istituto di Nanotecnologia UOS Cosenza, Università della Calabria, 87036 Arcavacata di Rende, CS, Italy;* orcid.org/0000-0002-8611-5575

Giuseppe Di Maio − *MAT-InLAB, LASCAMM CR-INSTM, Unità INSTM della Calabria, Dipartimento di Chimica e Tecnologie Chimiche, Università della Calabria, 87036 Arcavacata di Rende, CS, Italy*

Nicolas Godbert − *MAT-InLAB, LASCAMM CR-INSTM, Unità INSTM della Calabria, Dipartimento di Chimica e Tecnologie Chimiche, Università della Calabria, 87036 Arcavacata di Rende, CS, Italy; Laboratorio Preparazione Materiali, Star-Lab, Università della Calabria, 87036 Arcavacata di Rende, CS, Italy;* orcid.org/0000-0002-5659-8844

Antonio Tagarelli − *Dipartimento di Chimica e Tecnologie Chimiche, Università della Calabria, 87036 Arcavacata di Rende, CS, Italy*

Rosangela Elliani − *Dipartimento di Chimica e Tecnologie Chimiche, Università della Calabria, 87036 Arcavacata di Rende, CS, Italy*

Angela Candreva − *MAT-InLAB, LASCAMM CR-INSTM, Unità INSTM della Calabria, Dipartimento di Chimica e Tecnologie Chimiche and CNR-NANOTEC, Istituto di Nanotecnologia UOS Cosenza, Università della Calabria, 87036 Arcavacata di Rende, CS, Italy*

Renata De Rose − *Dipartimento di Chimica e Tecnologie Chimiche, Università della Calabria, 87036 Arcavacata di Rende, CS, Italy*

Iolinda Aiello − *MAT-InLAB, LASCAMM CR-INSTM, Unità INSTM della Calabria, Dipartimento di Chimica e Tecnologie Chimiche and CNR-NANOTEC, Istituto di Nanotecnologia UOS Cosenza, Università della Calabria, 87036 Arcavacata di Rende, CS, Italy; Laboratorio Preparazione Materiali, Star-Lab, Università della Calabria, 87036 Arcavacata di Rende, CS, Italy;* orcid.org/0000-0003-4804-2667

Mario Amati − *Dipartimento di Scienze, Università degli Studi della Basilicata, 85100 Potenza, Italy*

Complete contact information is available at: https://pubs.acs.org/10.1021/acs.cgd.3c00042

Notes

The authors declare no competing financial interest.

■ ACKNOWLEDGMENTS

This work was supported by the Programma Operativo Regionale (POR) Calabria FESR-FSE 2014/2020 and the project PON "Ricerca e Innovazione" 2014-2020, Progetto STAR 2, PIR01_00008, funded by MIUR (Ministero dell'Università e della Ricerca). F.S. is grateful to the project PON "Ricerca e Innovazione" 2014−2020, Asse IV "Istruzione e ricerca per il recupero," and Azione IV.6 "Contratti di ricerca su tematiche Green" (CUP: H25F21001230004; identification code: 1062_R8_GREEN).

■ REFERENCES

(1) Musgrave, R. A.; Russell, A. D.; Hayward, D. W.; Whittell, G. R.; Lawrence, P. G.; Gates, P. J.; Green, J. C.; Manners, I. Main-Chain Metallopolymers at the Static-Dynamic Boundary Based on Nickelocene. *Nat. Chem.* **2017**, *9*, 743−750.

(2) Eloi, J. C.; Chabanne, L.; Whittell, G. R.; Manners, I. Metallopolymers with Emerging Applications. *Mater. Today* **2008**, *11*, 28−36.

(3) Mauro, M.; Bellemin-Laponnaz, S.; Cebrián, C. Metal-Containing Polymers as Light-Emitting and Light-Responsive Materials and Beyond. *Chem. - A Eur. J.* **2017**, *23*, 17626−17636.

(4) Wang, Y.; Astruc, D.; Abd-El-Aziz, A. S. Metallopolymers for Advanced Sustainable Applications. *Chem. Soc. Rev.* **2019**, *48*, 558−636.

(5) Dzhardimalieva, G. I.; Rabinskiy, L. N.; Kydralieva, K. A.; Uflyand, I. E. Recent Advances in Metallopolymer-Based Drug Delivery Systems. *RSC Adv.* **2019**, *9*, 37009−37051.
(6) Yan, Y.; Zhang, J.; Ren, L.; Tang, C. Metal-Containing and Related Polymers for Biomedical Applications. *Chem. Soc. Rev.* **2016**, *45*, 5232−5263.
(7) Bentz, K. C.; Cohen, S. M. Supramolecular Metallopolymers: From Linear Materials to Infinite Networks. *Angew. Chem., Int. Ed.* **2018**, *57*, 14992−15001.
(8) Li, N.; Feng, R.; Zhu, J.; Chang, Z.; Bu, X. H. Conformation Versatility of Ligands in Coordination Polymers: From Structural Diversity to Properties and Applications. *Coord. Chem. Rev.* **2018**, *375*, 558−586.
(9) Rubio-Martinez, M.; Avci-Camur, C.; Thornton, A. W.; Imaz, I.; Maspoch, D.; Hill, M. R. New Synthetic Routes towards MOF Production at Scale. *Chem. Soc. Rev.* **2017**, *46*, 3453−3480.
(10) Viciano-Chumillas, M.; Mon, M.; Ferrando-Soria, J.; Corma, A.; Leyva-Pérez, A.; Armentano, D.; Pardo, E. Metal-Organic Frameworks as Chemical Nanoreactors: Synthesis and Stabilization of Catalytically Active Metal Species in Confined Spaces. *Acc. Chem. Res.* **2020**, 520.
(11) Wyszogrodzka, G.; Marszałek, B.; Gil, B.; Dorozyński, P. Metal-Organic Frameworks: Mechanisms of Antibacterial Action and Potential Applications. *Drug Discovery Today* **2016**, *21*, 1009−1018.
(12) Liu, A.; Wang, C. C.; Wang, C. Z.; Fu, H. F.; Peng, W.; Cao, Y. L.; Chu, H. Y.; Du, A. F. Selective Adsorption Activities toward Organic Dyes and Antibacterial Performance of Silver-Based Coordination Polymers. *J. Colloid Interface Sci.* **2018**, *512*, 730−739.
(13) Liu, J. Q.; Luo, Z. D.; Pan, Y.; Kumar Singh, A.; Trivedi, M.; Kumar, A. Recent Developments in Luminescent Coordination Polymers: Designing Strategies, Sensing Application and Theoretical Evidences. *Coord. Chem. Rev.* **2020**, *406*, No. 213145.
(14) Lawson, H. D.; Walton, S. P.; Chan, C. Metal-Organic Frameworks for Drug Delivery: A Design Perspective. *ACS Appl. Mater. Interfaces* **2021**, *13*, 7004−7020.
(15) Leong, W. L.; Vittal, J. J. One-Dimensional Coordination Polymers: Complexity and Diversity in Structures, Properties, and Applications. *Chem. Rev.* **2011**, *111*, 688−764.
(16) Loukopoulos, E.; Kostakis, G. E. Review: Recent Advances of One-Dimensional Coordination Polymers as Catalysts. *J. Coord. Chem.* **2018**, *71*, 371−410.
(17) Zhu, H.; Liu, D.; Li, Y. H.; Cui, G. H. A 1D Silver(I) Coordination Polymer as Luminescent Probe for Cu2+ and Effective Photocatalyst for Degradation Organic Dyes. *Inorg. Chem. Commun.* **2019**, *108*, No. 107539.
(18) Mondal, S.; Dastidar, P. Zn(II)-Coordination Polymers with a Right- And Left-Handed Twist: Multifunctional Metal-Organic Hybrid for Dye Adsorption and Drug Delivery. *Cryst. Growth Des.* **2020**, *20*, 7411−7420.
(19) Medici, S.; Peana, M.; Crisponi, G.; Nurchi, V. M.; Lachowicz, J. I.; Remelli, M.; Zoroddu, M. A. Silver Coordination Compounds: A New Horizon in Medicine. *Coord. Chem. Rev.* **2016**, *327*−*328*, 349−359.
(20) Lin, I. W. S.; Lok, C. N.; Yan, K.; Che, C. M. A Silver Complex of N, N′-Disubstituted Cyclic Thiourea as an Anti-Inflammatory Inhibitor of IκB Kinase. *Chem. Commun.* **2013**, *49*, 3297−3299.
(21) Scarpelli, F.; Crispini, A.; Giorno, E.; Marchetti, F.; Pettinari, R.; Di Nicola, C.; De Santo, M. P.; Fuoco, E.; Berardi, R.; Alfano, P.; Caputo, P.; Policastro, D.; Oliviero Rossi, C.; Aiello, I. Preparation and Characterization of Silver(I) Ethylcellulose Thin Films as Potential Food Packaging Materials. *Chempluschem* **2020**, *85*, 426−440.
(22) Teyssot, M.-L.; Jarrousse, A.-S.; Manin, M.; Chevry, A.; Roche, S.; Norre, F.; Beaudoin, C.; Morel, L.; Boyer, D.; Mahiou, R.; Gautier, A. Metal-NHC Complexes: A Survey of Anti-Cancer Properties. *Dalton Trans.* **2009**, *35*, 6894.
(23) Hemmert, C.; Fabié, A.; Fabre, A.; Benoit-Vical, F.; Gornitzka, H. Synthesis, Structures, and Antimalarial Activities of Some Silver(I), Gold(I) and Gold(III) Complexes Involving N-Heterocyclic Carbene Ligands. *Eur. J. Med. Chem.* **2013**, *60*, 64−75.
(24) Kalinowska-Lis, U.; Szewczyk, E. M.; Chęcińska, L.; Wojciechowski, J. M.; Wolf, W. M.; Ochocki, J. Synthesis, Characterization, and Antimicrobial Activity of Silver(I) and Copper-(II) Complexes of Phosphate Derivatives of Pyridine and Benzimidazole. *ChemMedChem* **2014**, *9*, 169−176.
(25) Bellusci, A.; Ghedini, M.; Giorgini, L.; Gozzo, F.; Szerb, E. I.; Crispini, A.; Pucci, D. Anion Dependent Mesomorphism in Coordination Networks Based on 2,2′-Bipyridine Silver(i) Complexes. *Dalt. Trans.* **2009**, *36*, 7381−7389.
(26) Khlobystov, A. N.; Blake, A. J.; Champness, N. R.; Lemenovskii, D. A.; Majouga, A. G.; Zyk, N. V.; Schröder, M. Supramolecular Design of One-Dimensional Coordination Polymers Based on Silver(I) Complexes of Aromatic Nitrogen-Donor Ligands. *Coord. Chem. Rev.* **2001**, *222*, 155−192.
(27) Kordestani, N.; Rudbari, H. A.; Fateminia, Z.; Caljon, G.; Maes, L.; Mineo, P. G.; Cordaro, A.; Mazzaglia, A.; Scala, A.; Micale, N. Antimicrobial and Antiprotozoal Activities of Silver Coordination Polymers Derived from the Asymmetric Halogenated Schiff Base Ligands. *Appl. Organomet. Chem.* **2020**, *2020*, 1−14.
(28) Lu, X.; Ye, J.; Sun, Y.; Bogale, R. F.; Zhao, L.; Tian, P.; Ning, G. Ligand Effects on the Structural Dimensionality and Antibacterial Activities of Silver-Based Coordination Polymers. *Dalton Trans.* **2014**, *43*, 10104−10113.
(29) Fromm, K. M. Silver Coordination Compounds with Antimicrobial Properties. *Appl. Organomet. Chem.* **2013**, *27*, 683−687.
(30) Kordestani, N.; Rudbari, H. A.; Fateminia, Z.; Caljon, G.; Maes, L.; Mineo, P. G.; Cordaro, A.; Mazzaglia, A.; Scala, A.; Micale, N. Antimicrobial and Antiprotozoal Activities of Silver Coordination Polymers Derived from the Asymmetric Halogenated Schiff Base Ligands. *Appl. Organomet. Chem.* **2021**, *35*, 1−14.
(31) Steed, J. W. The Role of Co-Crystals in Pharmaceutical Design. *Trends Pharmacol. Sci.* **2013**, *34*, 185−193.
(32) Spizzirri, U. G.; Carullo, G.; De Cicco, L.; Crispini, A.; Scarpelli, F.; Restuccia, D.; Aiello, F. Synthesis and Characterization of a (+)-Catechin and L-(+)-Ascorbic Acid Cocrystal as a New Functional Ingredient for Tea Drinks. *Heliyon* **2019**, *5*, No. e02291.
(33) Lu, B.; Fang, X.; Yan, D. Luminescent Polymorphic Co-Crystals: A Promising Way to the Diversity of Molecular Assembly, Fluorescence Polarization, and Optical Waveguide. *ACS Appl. Mater. Interfaces* **2020**, *12*, 31940−31951.
(34) Christopherson, J. C.; Topić, F.; Barrett, C. J.; Friščić, T. Halogen-Bonded Cocrystals as Optical Materials: Next-Generation Control over Light-Matter Interactions. *Cryst. Growth Des.* **2018**, *18*, 1245−1259.
(35) Khan, A.; Wang, M.; Usman, R.; Sun, H.; Du, M.; Xu, C. Molecular Marriage via Charge Transfer Interaction in Organic Charge Transfer Co-Crystals toward Solid-State Fluorescence Modulation. *Cryst. Growth Des.* **2017**, *17*, 1251−1257.
(36) Chappa, P.; Maruthapillai, A.; Voguri, R.; Dey, A.; Ghosal, S.; Basha, M. A. Drug-Polymer Co-Crystals of Dapsone and Polyethylene Glycol: An Emerging Subset in Pharmaceutical Co-Crystals. *Cryst. Growth Des.* **2018**, *18*, 7590−7598.
(37) Zhong, Z.; Guo, C.; Chen, L.; Xu, J.; Huang, Y. Co-Crystal Formation between Poly(Ethylene Glycol) and a Small Molecular Drug Griseofulvin. *Chem. Commun.* **2014**, *50*, 6375−6378.
(38) Ganesh, M.; Ubaidulla, U.; Rathnam, G.; Jang, H. T. Chitosan-Telmisartan Polymeric Cocrystals for Improving Oral Absorption: In Vitro and in Vivo Evaluation. *Int. J. Biol. Macromol.* **2019**, *131*, 879−885.
(39) Mukherjee, P.; Drew, M. G. B.; Gómez-García, C. J.; Ghosh, A. (Ni2), (Ni3), and (Ni2 + Ni3): A Unique Example of Isolated and Cocrystallized Ni2 and Ni 3 Complexes. *Inorg. Chem.* **2009**, *48*, 4817−4827.
(40) Datta, J.; Nandi, A. K. Cocrystallization of Poly(Vinylidene Fluoride) and Vinylidene Fluoride-Tetrafluoroethylene Copolymers: 1. Effect of Chain Structure and Crystallization Conditions. *Polymer* **1994**, *35*, 4804−4812.

https://doi.org/10.1021/acs.cgd.3c00042
Cryst. Growth Des. 2023, 23, 3518−3534

(41) Thakur, T. S.; Thakuria, R. Crystalline Multicomponent Solids: An Alternative for Addressing the Hygroscopicity Issue in Pharmaceutical Materials. *Cryst. Growth Des.* **2020**, *20*, 6245−6265.
(42) Shaffer, C. C.; Liu, W.; Oliver, A. G.; Smith, B. D. Supramolecular Paradigm for Capture and Co-Precipitation of Gold(III) Coordination Complexes. *Chem. - A Eur. J.* **2021**, *27*, 751−757.
(43) Gao, X. S.; Dai, H. J.; Tang, Y.; Ding, M. J.; Pei, W. B.; Ren, X. M. Crystal Structures, Photoluminescence, and Magnetism of Two Novel Transition-Metal Complex Cocrystals with Three-Dimensional H-Bonding Organic Framework or Alternating Noncovalent Anionic and Cationic Layers. *ACS Omega* **2019**, *4*, 12230−12237.
(44) Hadadzadeh, H.; Mansouri, G.; Rezvani, A. R.; Khavasi, H. R. A Novel 1:1 Co-Crystal of Bis(1,10-Phenanthroline) (1,10-Phenanthroline-5, 6-Dione)Nickel(II) Hexafluorophosphate and Tris(1,10-Phenanthroline)Nickel(II) Hexafluorophosphate Complexes, [Ni-(Phen) 2(Phen-Dione)] [Ni(Phen) 3] (PF 6) 4. *J. Chem. Crystallogr.* **2012**, *42*, 486−493.
(45) Golbedaghi, R.; Salehzadeh, S.; Khavasi, H. R.; Blackman, A. G. Mn(II) Complexes of Three [2 + 2] Macrocyclic Schiff Base Ligands. Synthesis and X-Ray Crystal Structure of the First Binuclear-Di(Binuclear) Cocrystal. *Polyhedron* **2014**, *68*, 151−156.
(46) Nayak, M.; Jana, A.; Fleck, M.; Hazra, S.; Mohanta, S. A Unique Example of a Three Component Cocrystal of Metal Complexes. *CrystEngComm* **2010**, *12*, 1416−1421.
(47) Das, L. K.; Biswas, A.; Gómez-García, C. J.; Drew, M. G. B.; Ghosh, A. Isolation of Two Different Ni2Zn Complexes with an Unprecedented Cocrystal Formed by One of Them and a "Coordination Positional Isomer" of the Other. *Inorg. Chem.* **2014**, *53*, 434−445.
(48) Scarpelli, F.; La Deda, M.; Godbert, N.; Marino, N.; Crispini, A.; Aiello, I. The Strange Case of Metal Coordination in Disubstituted-Biquinolines: Competition between Ligands and Formation of a Hybrid Organic/Inorganic Cu(II)/Cu(I) Ternary Cocrystal. *J. Coord. Chem.* **2022**, *75*, 2448−2470.
(49) Purcell, W.; Basson, S. S.; Leipoldt, J. G.; Roodt, A.; Preston, H. First Structural Confirmation of Different Geometrical Isomers in the Same Crystal Lattice: The Crystal Structure of Benzoylacetonato-carbonyltriphenylphosphinerhodium(I). *Inorganica Chim. Acta* **1995**, *234*, 153−156.
(50) Bellusci, A.; Crispini, A.; Pucci, D.; Szerb, E. I.; Ghedini, M. Structural Variations in Bipyridine Silver(i) Complexes: Role of the Substituents and Counterions. *Cryst. Growth Des.* **2008**, *8*, 3114−3122.
(51) Hung-Low, F.; Renz, A.; Klausmeyer, K. K. An X-Ray Diffraction Study of Anion and Ratio Dependence in the Formation of Discrete Molecules versus Polymeric Arrays Involving Silver Salts and Bipyridine Ligands. *Polyhedron* **2009**, *28*, 407−415.
(52) Sun, J. K.; Yang, X. D.; Yang, G. Y.; Zhang, J. Bipyridinium Derivative-Based Coordination Polymers: From Synthesis to Materials Applications. *Coord. Chem. Rev.* **2019**, *378*, 533−560.
(53) Gupta, N.; Verma, K.; Nalla, S.; Kulshreshtha, A.; Lall, R.; Prasad, S. Free Radicals as a Double-Edged Sword: The Cancer Preventive and Therapeutic Roles of Curcumin. *Molecules* **2020**, *25*, 1−20.
(54) Zheng, D.; Huang, C.; Huang, H.; Zhao, Y.; Khan, M. R. U.; Zhao, H.; Huang, L. Antibacterial Mechanism of Curcumin: A Review. *Chem. Biodiversity* **2020**, DOI: 10.1002/cbdv.202000171.
(55) Hewlings, S.; Kalman, D. Curcumin: A Review of Its Effects on Human Health. *Foods* **2017**, *6*, 92.
(56) Sanphui, P.; Goud, N. R.; Khandavilli, U. B. R.; Bhanoth, S.; Nangia, A. New Polymorphs of Curcumin. *Chem. Commun.* **2011**, *47*, 5013.
(57) Sanphui, P.; Goud, N. R.; Khandavilli, U. B. R.; Nangia, A. Fast Dissolving Curcumin Cocrystals. *Cryst. Growth Des.* **2011**, *11*, 4135−4145.
(58) Rathi, N.; Paradkar, A.; Gaikar, V. G. Polymorphs of Curcumin and Its Cocrystals With Cinnamic Acid. *J. Pharm. Sci.* **2019**, *108*, 2505−2516.
(59) Wong, S. N.; Hu, S.; Ng, W. W.; Xu, X.; Lai, K. L.; Lee, W. Y. T.; Chow, A. H. L.; Sun, C. C.; Chow, S. F. Cocrystallization of Curcumin with Benzenediols and Benzenetriols via Rapid Solvent Removal. *Cryst. Growth Des.* **2018**, *18*, 5534−5546.
(60) Dal Magro, C.; dos Santos, A. E.; Ribas, M. M.; Aguiar, G. P. S.; Volfe, C. R. B.; Lopes, M. L. L. C.; Siebel, A. M.; Müller, L. G.; Bortoluzzi, A. J.; Lanza, M.; Oliveira, J. V. Production of Curcumin-Resveratrol Cocrystal Using Cocrystallization with Supercritical Solvent. *J. Supercrit. Fluids* **2021**, *171*, No. 105190.
(61) Bruker. SAINT. Madison, WI: Bruker AXS Inc. 2003.
(62) Sheldrick, G. M. *SADABS Empirical Absorption Program*. 2003.
(63) Sheldrick, G. M. A Short History of SHELX. *Acta Crystallogr. Sect. A Found. Crystallogr.* **2008**, *64*, 112−122.
(64) Sheldrick, G. M. Crystal Structure Refinement with SHELXL. *Acta Crystallogr. Sect. C Struct. Chem.* **2015**, *71*, 3−8.
(65) Müller, P. Practical Suggestions for Better Crystal Structures. *Crystallogr. Rev.* **2009**, *15*, 57−83.
(66) Dolomanov, O. V.; Bourhis, L. J.; Gildea, R. J.; Howard, J. A. K.; Puschmann, H. OLEX2 : A Complete Structure Solution, Refinement and Analysis Program. *J. Appl. Crystallogr.* **2009**, *42*, 339−341.
(67) Macrae, C. F.; Sovago, I.; Cottrell, S. J.; Galek, P. T. A.; McCabe, P.; Pidcock, E.; Platings, M.; Shields, G. P.; Stevens, J. S.; Towler, M.; Wood, P. A. Mercury 4.0 : From Visualization to Analysis, Design and Prediction. *J. Appl. Crystallogr.* **2020**, *53*, 226−235.
(68) Ionescu, A.; Godbert, N.; Ricciardi, L.; La Deda, M.; Aiello, I.; Ghedini, M.; Rimoldi, I.; Cesarotti, E.; Facchetti, G.; Mazzeo, G.; Longhi, G.; Abbate, S.; Fusè, M. Luminescent Water-Soluble Cycloplatinated Complexes: Structural, Photophysical, Electrochemical and Chiroptical Properties. *Inorganica Chim. Acta* **2017**, *461*, 267−274.
(69) Frisch, M. J.; Trucks, G. W.; Schlegel, H. B.; Scuseria, G. E.; Robb, M. A.; Cheeseman, J. R.; Scalmani, G.; Barone, V.; Mennucci, B.; Petersson, G. A.; Nakatsuji, H.; Caricato, M.; Li, X.; Hratchian, H. P.; Izmaylov, A. F.; Bloino, J.; Zheng, G.; Sonnenb, D. J. *Gaussian 09*, Revision D.01. Gaussian, Inc.: Wallingford CT 2010.
(70) Becke, A. D. A New Mixing of Hartree−Fock and Local Density-functional Theories. *J. Chem. Phys.* **1993**, *98*, 1372−1377.
(71) Weigend, F.; Ahlrichs, R. Balanced Basis Sets of Split Valence, Triple Zeta Valence and Quadruple Zeta Valence Quality for H to Rn: Design and Assessment of Accuracy. *Phys. Chem. Chem. Phys.* **2005**, *7*, 3297.
(72) ADF2019, SCM, *Theoretical Chemistry*, Vrije Universiteit, Amsterdam, The Netherlands, Http://Www.Scm.Com.
(73) te Velde, G.; Bickelhaupt, F. M.; Baerends, E. J.; Fonseca Guerra, C.; van Gisbergen, S. J. A.; Snijders, J. G.; Ziegler, T. Chemistry with ADF. *J. Comput. Chem.* **2001**, *22*, 931−967.
(74) Fonseca Guerra, C.; Snijders, J. G.; te Velde, G.; Baerends, E. J. Towards an Order- N DFT Method. *Theor. Chem. Acc.* **1998**, *99*, 391−403.
(75) van Lenthe, E.; Baerends, E. J.; Snijders, J. G. Relativistic Regular Two-component Hamiltonians. *J. Chem. Phys.* **1993**, *99*, 4597−4610.
(76) van Lenthe, E.; Baerends, E. J.; Snijders, J. G. Relativistic Total Energy Using Regular Approximations. *J. Chem. Phys.* **1994**, *101*, 9783−9792.
(77) Ziegler, T.; Rauk, A. On the Calculation of Bonding Energies by the Hartree Fock Slater Method. *Theor. Chim. Acta* **1977**, *46*, 1−10.
(78) Kitaura, K.; Morokuma, K. A New Energy Decomposition Scheme for Molecular Interactions within the Hartree-Fock Approximation. *Int. J. Quantum Chem.* **1976**, *10*, 325−340.
(79) Zhao, Y.; Truhlar, D. G. The M06 Suite of Density Functionals for Main Group Thermochemistry, Thermochemical Kinetics, Noncovalent Interactions, Excited States, and Transition Elements: Two New Functionals and Systematic Testing of Four M06-Class Functionals and 12 Other Function. *Theor. Chem. Acc.* **2008**, *120*, 215−241.

(80) Grimme, S.; Antony, J.; Ehrlich, S.; Krieg, H. A Consistent and Accurate Ab Initio Parametrization of Density Functional Dispersion Correction (DFT-D) for the 94 Elements H-Pu. *J. Chem. Phys.* **2010**, *132*, 154104.
(81) Beheshti, A.; Zafarian, H. R.; Khorramdin, R.; Fattahi Monavvar, M.; Abrahams, C. T. Novel Silver(I) Pyrazole-Based Coordination Polymers: Synthetic and Structural Studies. *Polyhedron* **2012**, *48*, 245−252.
(82) Vitõrica-Yrezábal, I. J.; Libri, S.; Loader, J. R.; Mínguez Espallargas, G.; Hippler, M.; Fletcher, A. J.; Thompson, S. P.; Warren, J. E.; Musumeci, D.; Ward, M. D.; Brammer, L. Coordination Polymer Flexibility Leads to Polymorphism and Enables a Crystalline Solid-Vapour Reaction: A Multi-Technique Mechanistic Study. *Chem. - A Eur. J.* **2015**, *21*, 8799−8811.
(83) Kulovi, S.; Pradhan, A.; Maiti, S.; Puschmann, H.; Zangrando, E.; Dalai, S. Polymorphism in [Ag(Bpetan)]n Coordination Polymers with Nitrate and Isophthalate Anions: Photocatalytic and Antibacterial Activity, Hemolysis Assay and Study of Cytotoxicity. *ChemistrySelect* **2020**, *5*, 3337−3346.
(84) Robin, A. Y.; Sague Doimeadios, J. L.; Neels, A.; Vig Slenters, T.; Fromm, K. M. Structure-Property Relationships: Polymorphism, Solvates, and Clay Behavior in the One-Dimensional Coordination Polymer Chains [Ag(L)(NO3)](H2O)n, L = Ethanediyl Bis-(Isonicotinate), n = 0, and 2. *Inorganica Chim. Acta* **2007**, *360*, 212−220.
(85) Janasi, S. R.; Rodrigues, D.; Emura, M.; Landgraf, F. J. G. Barium Ferrite Powders Obtained by Co-Precipitation. *Phys. Status Solidi Appl. Res.* **2001**, *185*, 479−485.
(86) Newman, A. Specialized Solid Form Screening Techniques. *Org. Process Res. Dev.* **2013**, *17*, 457−471.
(87) Kuzmicheva, G. M.; Savinkina, E. V.; Obolenskaya, L. N.; Zubavichus, Y. V.; Murzin, V. Y.; Podbelskiy, V. V.; Sadovskaya, N. V. Synthesis of Mn-Sensitized TiO 2 Nanoparticles: Influence of Sequence of Reagents on Phase Composition and Photocatalytic Activity. *J. Nanopart. Res.* **2015**, *17*, 1−12.
(88) Argyle, V. J.; Woods, L. M.; Roxburgh, M.; Hanton, L. R. Triflate Anion and Ligand Influences in Silver(i) Coordination Polymers of Four Isomeric Dipyridyl Ketone Oximes. *CrystEngComm* **2013**, *15*, 120−134.
(89) Syed, H. K.; Iqbal, M. A.; Haque, R. A.; Peh, K. K. Synthesis, Characterization and Antibacterial Activity of a Curcumin-Silver(I) Complex. *J. Coord. Chem.* **2015**, *68*, 1088−1100.
(90) Sanphui, P.; Bolla, G. Curcumin, a Biological Wonder Molecule: A Crystal Engineering Point of View. *Cryst. Growth Des.* **2018**, *18*, 5690−5711.
(91) Sathisaran, I.; Dalvi, S. V. Crystal Engineering of Curcumin with Salicylic Acid and Hydroxyquinol as Coformers. *Cryst. Growth Des.* **2017**, *17*, 3974−3988.
(92) Verma, A. D.; Jain, N.; Singha, S. K.; Quraishi, M. A.; Sinha, I. Green Synthesis and Catalytic Application of Curcumin Stabilized Silver Nanoparticles. *J. Chem. Sci.* **2016**, *128*, 1871−1878.
(93) Gupta, A.; Briffa, S. M.; Swingler, S.; Gibson, H.; Kannappan, V.; Adamus, G.; Kowalczuk, M.; Martin, C.; Radecka, I. Synthesis of Silver Nanoparticles Using Curcumin-Cyclodextrins Loaded into Bacterial Cellulose-Based Hydrogels for Wound Dressing Applications. *Biomacromolecules* **2020**, *21*, 1802−1811.
(94) Khan, M. J.; Shameli, K.; Sazili, A. Q.; Selamat, J.; Kumari, S. Rapid Green Synthesis and Characterization of Silver Nanoparticles Arbitrated by Curcumin in an Alkaline Medium. *Molecules* **2019**, *24*, 719.
(95) Soto-Quintero, A.; Guarrotxena, N.; García, O.; Quijada-Garrido, I. Curcumin to Promote the Synthesis of Silver NPs and Their Self-Assembly with a Thermoresponsive Polymer in Core-Shell Nanohybrids. *Sci. Rep.* **2019**, *9*, 1−14.
(96) Kumavat, S. D.; Chaudhari, Y. S.; Borole, P.; Mishra, P.; Shenghani, K.; Duvvuri, P. Degradation Studies of Curcumin. *Int. J. Pharm. Rev. Res.* **2013**, *3*, 50−55.
(97) Schneider, C.; Gordon, O. N.; Edwards, R. L.; Luis, P. B. Degradation of Curcumin: From Mechanism to Biological Implications. *J. Agric. Food Chem.* **2015**, *63*, 7606−7614.
(98) Jankun, J.; Wyganowska-Swiatkowska, M.; Dettlaff, K.; JelinSka, A.; Surdacka, A.; Watróbska-Swietlikowska, D.; Skrzypczak-Jankun, E. Determining Whether Curcumin Degradation/Condensation Is Actually Bioactivation (Review). *Int. J. Mol. Med.* **2016**, *37*, 1151−1158.
(99) Kharat, M.; Du, Z.; Zhang, G.; McClements, D. J. Physical and Chemical Stability of Curcumin in Aqueous Solutions and Emulsions: Impact of PH, Temperature, and Molecular Environment. *J. Agric. Food Chem.* **2017**, *65*, 1525−1532.
(100) Zhao, X. Z.; Jiang, T.; Wang, L.; Yang, H.; Zhang, S.; Zhou, P. Interaction of Curcumin with Zn(II) and Cu(II) Ions Based on Experiment and Theoretical Calculation. *J. Mol. Struct.* **2010**, *984*, 316−325.
(101) Priyadarsini, K. I. The Chemistry of Curcumin: From Extraction to Therapeutic Agent. *Molecules* **2014**, *19*, 20091−20112.
(102) Zhu, J.; Sanidad, K. Z.; Sukamtoh, E.; Zhang, G. Potential Roles of Chemical Degradation in the Biological Activities of Curcumin. *Food Funct.* **2017**, *8*, 907−914.
(103) Mohan, P. R. K.; Sreelakshmi, G.; Muraleedharan, C. V.; Joseph, R. Water Soluble Complexes of Curcumin with Cyclodextrins: Characterization by FT-Raman Spectroscopy. *Vib. Spectrosc.* **2012**, *62*, 77−84.
(104) Tayyari, S. F.; Zeegers-Huyskens, T.; Wood, J. L. Spectroscopic Study of Hydrogen Bonding in the Enol Form of β-Diketones—I. Vibrational Assignment and Strength of the Bond. *Spectrochim. Acta, Part A* **1979**, *35*, 1265−1276.
(105) Chiavassa, T.; Verlaque, P.; Pizzala, L.; Roubin, P. Vibrational Studies of Methyl Derivatives of Malonaldehyde: Determination of a Reliable Force Field for β-Dicarbonyl Compounds. *Spectrochim. Acta, Part A* **1994**, *50*, 343−351.
(106) Hansen, P. E.; Spanget-Larsen, J. NMR and IR Investigations of Strong Intramolecular Hydrogen Bonds. *Molecules* **2017**, *22*, 552.
(107) Subhan, M. A.; Alam, K.; Rahaman, M. S.; Rahman, M. A.; Awal, R. Synthesis and Characterization of Metal Complexes Containing Curcumin ($C_{21}H_{20}O_6$) and Study of Their Anti-Microbial Activities and DNA-Binding Properties. *J. Sci. Res.* **2014**, *6*, 97−109.
(108) Frei, A.; Zuegg, J.; Elliott, A. G.; Baker, M.; Braese, S.; Brown, C.; Chen, F. G.; Dowson, C.; Dujardin, G.; Jung, N.; King, A. P.; Mansour, A. M.; Massi, M.; Moat, J.; Mohamed, H. A.; Renfrew, A. K.; Rutledge, P. J.; Sadler, P. J.; Todd, M. H.; Willans, C. E.; Wilson, J. J.; Cooper, M. A.; Blaskovich, M. A. T. Metal Complexes as a Promising Source for New Antibiotics. *Chem. Sci.* **2020**, *11*, 2627−2639.
(109) Lu, X.; Ye, J.; Zhang, D.; Xie, R.; Bogale, R. F.; Sun, Y.; Zhao, L.; Zhao, Q.; Ning, G. Silver Carboxylate Metal-Organic Frameworks with Highly Antibacterial Activity and Biocompatibility. *J. Inorg. Biochem.* **2014**, *138*, 114−121.
(110) Manolova, Y.; Deneva, V.; Antonov, L.; Drakalska, E.; Momekova, D.; Lambov, N. The Effect of the Water on the Curcumin Tautomerism: A Quantitative Approach. *Spectrochim. Acta Part A* **2014**, *132*, 815−820.
(111) Kolev, T. M.; Velcheva, E. A.; Stamboliyska, B. A.; Spiteller, M. DFT and Experimental Studies of the Structure and Vibrational Spectra of Curcumin. *Int. J. Quantum Chem.* **2005**, *102*, 1069−1079.

https://doi.org/10.1021/acs.cgd.3c00042
Cryst. Growth Des. 2023, 23, 3518−3534